# 平成２５年度
# 同軸２重反転式小型無人ヘリコプタの運動解析
# 報告書

提出日：26 年 3 月 31 日

作成者: 鈴木智

この研究はオートレースの補助によって行いました.

http://ringring-keirin.jp/

## 1. 本研究の目的

本研究では，同軸二重反転式小型無人ヘリコプタの解析，性能向上，及び自律制御を行い，農林業や防災・災害支援等に幅広く応用可能な有人・無人ヘリコプタの開発と評価を行うことを目的とする．

## 2. 本年度の研究目的と手順

本年度は，ヘリコプタ運動モデルの高精度化を図るとともに，モデルを用いた機体の運動解析を行うことを目的とする．具体的には，高精度化として，二重反転ロータ間の空気力学の詳細の解析及びモデルへの導入を行う．また，運動解析として，作成したモデルを用いたシミュレーションによって機体安定性と機体各部パラメータの関係性を明らかにする．

## 3. 研究概要及び結果

これまでの数式モデルで十分に考慮されていなかった 2 重反転ロータ間の空気力学の解析を行い，得られたロータダイナミクスをモデルに導入した．また、導出した数学モデルをコンピュータ上でシミュレーションできる環境を数値解析ソフトウェアである MATLAB を用いて構築した。構築したシミュレーション環境を用いた基礎的な運動解析を行った。詳細は別添 1 に示す．この研究はインド工科大学からインターンシップとして研究室を訪れた Puneet SINGH 君によって行われ、彼の研究成果を応用したものである。この解析によって固定ピッチ同軸二重反転ロータを用いた場合の巡航速度の理論的な限界値を明らかにすることができた．また，前進飛行時の機体挙動に対してロータブレードの剛性が大きく寄与しており，ロータ剛性が高いほど飛行時の横挙動が振動的になることが新たに明らかとなった．

## 4. まとめと今後の課題

25 年度の研究では，数式モデルの厳密化とモデルを用いた運動解析を行った．これによって様々な視点からの機体パラメータの検討を行うことが可能となった．今後は，得られた知見を実機体の設計にフィードバックするとともに今年度の研究結果の一部を随時論文化していく予定である．

# 別添１：同軸２重反転ロータ空気力学の解析

# GEN-H4 : Coaxial Rotor Helicopter

*Author:*
Puneet Singh

*Supervisor:*
Prof. Satoshi Suzuki

Department of Functional Machinery and Mechanics

Shinshu University, Ueda, Nagano, Japan

# Abstract

The GEN Corporation in Japan has pioneered the development of a novel compact aerial vehicle known as the GEN-H4 helicopter. The vehicle uses two contra rotating coaxial rotors for flight. Although conventional single rotor helicopter dynamics has been widely studied, there has been little academic study done on coaxial rotors and their mutual interaction. Also, the rotor blades have a fixed pitch and do not have a swash plate mechanism like other helicopters. The control of the helicopters motion is achieved by tilting the rotor shaft and shifting weight. This further complicates the dynamics of the vehicle motion, as conventional helicopters are modeled as a single rigid body. Previous research at Shinshu University had developed a mechanical model of the unmanned version of the vehicle. The present study aims to incorporate the rotor aerodynamics with the model, and include effects of the blade profile and motion of the helicopter on the forces and moments produced by the rotor.

# Acknowledgment

The work presented in this report was completed during a 10 week internship sponsored by the Honda Foundation in its YES Plus Award program. The author profusely thanks Ms.Eri Motoki, Mr. Noyori, Mr. Harada, and Mr. Matsuzawa for providing such great support and care in making this internship possible. I would also like to express my intense gratitude to Prof. Satoshi Suzuki, for being the most amazing professor one could hope for. His hard work, intelligence yet extremely friendly and caring attitude has inspired me a lot. Due to him I had the unique opportunity to interact with the GEN corporation. I was able to fulfill a dream of mine by being able to visit and interact with Mr. Gennai Yanagisawa, the creator of the GEN 4 Helicopter. I also am thankful to the students and teachers at Shinshu University, and staff of the GEN corporation. I am grateful to have made such good friends and hope to cherish their friendship my whole life. They have made this experience many times more memorable.

# Contents

# List of Figures

# List of Tables

# 1 Introduction

The GEN Corporation in Japan has developed a unique design for a helicopter known as the GEN-H4. The vehicle lifts with the aid of two contra rotating coaxial rotors. The torque generated by each rotor cancels out since the rotors rotate in opposite direction. This allows the vehicle to be have net zero yaw moment. Conventional single rotor helicopters use a tail rotor to cancel the torque of the single rotor. Hence they consume power which does not provide lift to the vehicle. The coaxial rotors on the other hand both produce thrust to lift the vehicle. They are therefore also much more compact than one single rotor to lift the same weight.

The two rotors are powered by four special lightweight engines manufactured by the GEN corporation. The aerodynamic environment of the two rotors is not the same, since the lower rotor is significantly affected by the down wash of the upper rotor. Therefore, the two rotors operate at different rotation speeds to correct the yaw moment. This is made possible by the differential gear box transmission to the coaxial shaft from the four engines. The four engines allow redundancy in case of any engine failure during flight. An electronic gyro sensor gives feedback to the engine control unit to change the rotation speeds of the rotors.

The four engines and the transmission are known as the 'Mission Unit'. This mission unit is pivoted about a hinge so that it can be tilted in any direction forwards or sidewards. This tilting is accomplished by the control bar in the manned version, or by servos in the unmanned version. Due to the tilt of the rotor, the thrust vector of the coaxial rotors is changed and provides a horizontal force for the vehicle's motion. In conventional helicopters, the shaft has a fixed direction with respect to the fuselage. The horizontal forces are produced by changing the flapping of the blades. This is done by changing the pitch angle of the blades, using a swash plate mechanism. This is a complicated mechanical assembly containing rotating and non rotating units. The GEN-H4 helicopter has fixed pitch rotor blades which eliminates the need for the intense maintenance associated with a rotor hub with a swash plate. However the dynamics of the vehicle are made complex due to shift in displacement and orientation of the mission unit during flight.

## 1.1 Previous Research

There is a lack of literature on coaxial rotor aerodynamics in general. The recent development of the Sikorsky X2 helicopter has increased research on such vehicles, but the unique design of the GEN-H4 sets it apart from them.

Previous work at Shinshu University on the GEN-H4 helicopter developed a mechanical model of the unmanned version of the vehicle using the Velocity Transformation Method. The vehicle was modeled as 4 separate rigid bodies: the 'Frame Unit', the 'Mission Unit', the upper rotor blades, and the lower rotor blades.

The rotor thrust was obtained using momentum theory for a constant chord and pitch angle blade. The blades were assumed to have a pre-cone flap angle. The root of the blade was assumed to have an angular spring and damper system to represent the elasticity of the flexible blade.

The results of the study showed an excellent match of the simulation with the experimental results.

## 1.2 Objectives of Research

Based on the previous work done at Shinshu University, the following aims were identified to achieve during the research period.

- Include effects of linear twist and taper of the blades on the aerodynamics
- Identify the blade stiffness and mass properties
- Introduce a non uniform inflow model on the rotor
- Conduct a preliminary stability and control analysis on the vehicle

## 1.3 Organization of Report

The report is organized in the following manner:

- Section 2 gives important details about the blade geometry, which is used to calculate important parameters of the blade mass distribution.
- Section 3 details the simple finite element analysis done to idealize the blade and validate the geometrical approximations made in the previous section.
- Section 3 gives a closed form solution of the rotor aerodynamic in forward flight.
- Section 4 integrates the rotor model with the mechanical motion of the body. The impact of the forward speed on the controls was studied.
- Section 5 contains a simple study of the stability and control response in hover.
- Section 6 gives a summary of the results of the study and discusses future work.

# 2 Blade Model

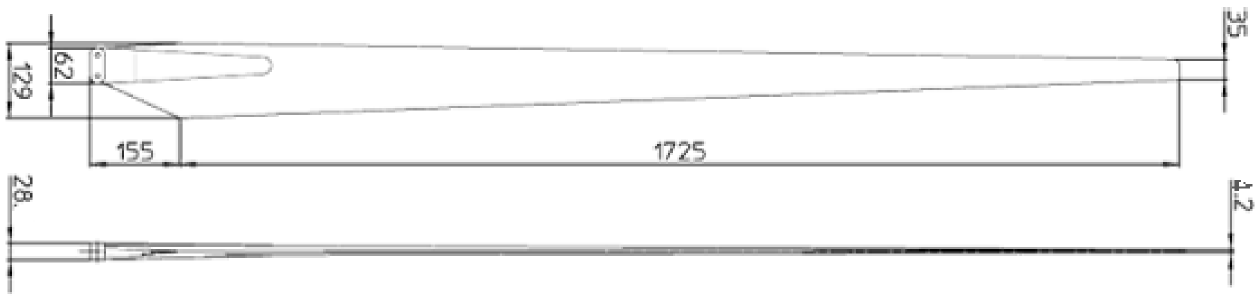


Figure 1: Blade Plan-form

The blade plan-form used on the vehicle is shown in Fig. 1. The net rotor radius of the vehicle is 2.0m. The length of the blade is 1.88m, while the rest is the attachment from the rotor shaft to the rotor blade .

The chord of the rotor blade from the root initially increases from 62 mm to 129 mm till a point 155 mm from the root. The chord then decreases to the tip to 35 mm. The thickness of the blade decreases uniformly from 28 mm at the root till 4.2 mm at the tip. The twist of the blade is linear and decreases by 6.4 degrees from the root to the tip. The blade pitch angle at a location 3/4th of the rotor radius from the shaft is 10 degrees.

## 2.1 Idealization

The rotor blade is idealized with an offset and a linear chord distribution as shown in Fig. 2. The ratio of the offset distance with respect to the rotor radius ($R$) is $e$. The radial location is non dimensionalized as $\bar{r} = r/R$. Hence the non dimensional radial location of the tip is given by:

$$\bar{r}_{tip} = \frac{L}{R} = \frac{R - offset}{R} = 1 - e$$

We can now define the chord distribution as:

$$c = c_0 + c_1\bar{r} \tag{1}$$

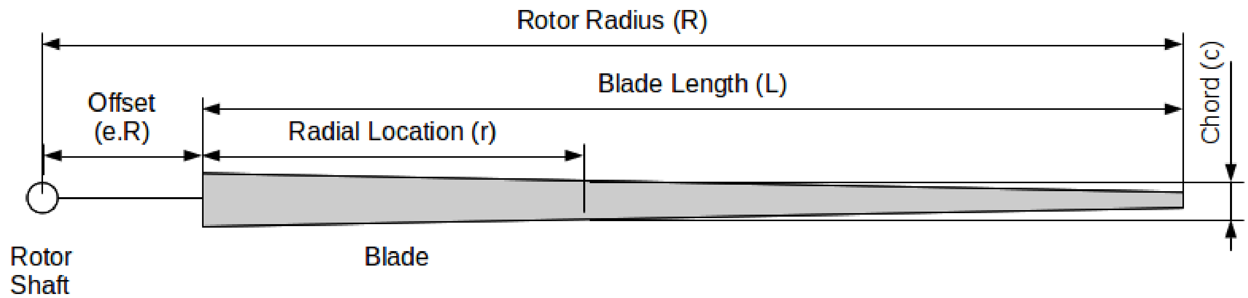


Figure 2: Blade Idealization

Also the the thickness distribution is defined as:

$$t = t_0 + t_1 \bar{r} \tag{2}$$

Similarly, the blade pitch angle is given as:

$$\theta = \theta_0 + \theta_1 \bar{r} \tag{3}$$

## 2.2 Mass

The total mass of the blade is 1.17 kg. This includes a concentrated mass at the tip. Hence the total mass can be written as:

$$m_{total} = m_{blade} + m_{tip} \tag{4}$$

The rest of the mass of the blade is assumed to be of uniform density. Therefore, the mass of the blade can be written as the following, where $\rho$ denotes density and $V$ denotes volume:

$$m_{blade} = \rho_{blade} V_{blade} \tag{5}$$

The cross-section of the blade is an airfoil. This shape is assumed to be constant over the complete blade. The area of the cross-section is assumed to be proportional to the product of the chord and thickness, with a constant shape coefficient $f_{airfoil}$:

$$f_{airfoil} = \frac{A_{airfoil}}{c.t} \tag{6}$$

The volume element at a radial location on the blade is the product of the area of cross-section with the elemental width:

$$dV_{blade} = A_{airfoil}.dr = f_{airfoil}.c.t.R.d\bar{r} \tag{7}$$

This is now integrated from the blade root to the tip to obtain the total volume:

$$V_{blade} = \int_0^{1-e} f_{airfoil}.c.t.R.d\bar{r} =$$

$$f_{airfoil}R\int_0^{1-e}(c_0 + c_1\bar{r}).(t_0 + t_1\bar{r}).d\bar{r} = f_{airfoil}R\int_0^{1-e}[c_0t_0 + (c_1t_0 + c_0t_1)\bar{r} + c_1t_1\bar{r}^2].d\bar{r}$$

$$V_{blade} = f_{airfoil}R(1-e)\left[c_0t_0 + (c_1t_0 + c_0t_1)\frac{(1-e)}{2} + c_1t_1\frac{(1-e)^2}{3}\right] \tag{8}$$

## 2.3 Center of Gravity

The center of gravity of the total blade can be calculated as per the following method.

$$X_{cg,total} = \frac{\int_0^L r.dm}{m_{total}} = \frac{m_{blade}X_{cg,blade} + m_{tip}.L}{m_{blade} + m_{tip}} \tag{9}$$

The center of gravity of the uniformly distributed mass of the blade can be obtained as:

$$X_{cg,blade} = \frac{\rho_{blade}\int_0^L r.dV_{blade}}{m_{blade}} = \frac{\int_0^L r.dV_{blade}}{V_{blade}} \tag{10}$$

The integral in the numerator of the above expression is obtained as:

$$\int_0^L r.dV_{blade} = f_{airfoil}R^2\int_0^{1-e}\bar{r}(c_0 + c_1\bar{r}).(t_0 + t_1\bar{r}).d\bar{r}$$

$$= f_{airfoil}R^2\int_0^{1-e}[c_0t_0\bar{r} + (c_1t_0 + c_0t_1)\bar{r}^2 + c_1t_1\bar{r}^3].d\bar{r}$$

$$\int_0^L r.dV_{blade} = f_{airfoil}R^2\left[c_0t_0\frac{(1-e)^2}{2} + (c_1t_0 + c_0t_1)\frac{(1-e)^3}{3} + c_1t_1\frac{(1-e)^4}{4}\right] \tag{11}$$

Hence, the center of gravity of the blade is found to be:

$$X_{cg,blade} = R\left[\frac{c_0t_0\dfrac{(1-e)}{2} + (c_1t_0 + c_0t_1)\dfrac{(1-e)^2}{3} + c_1t_1\dfrac{(1-e)^3}{4}}{c_0t_0 + (c_1t_0 + c_0t_1)\dfrac{(1-e)}{2} + c_1t_1\dfrac{(1-e)^2}{3}}\right] \tag{12}$$

Note that this is only dependent on the geometry of the blade. We can now define the ratio of the tip mass and the blade mass as:

$$\mu_{tip} = \frac{m_{tip}}{m_{blade}} \tag{13}$$

Therefore, the net center of gravity of the blade can be found as:

$$X_{cg,total} = R(1-e)\frac{\left[\dfrac{\dfrac{c_0t_0}{2} + (c_1t_0 + c_0t_1)\dfrac{(1-e)}{3} + c_1t_1\dfrac{(1-e)^2}{4}}{c_0t_0 + (c_1t_0 + c_0t_1)\dfrac{(1-e)}{2} + c_1t_1\dfrac{(1-e)^2}{3}}\right] + \mu_{tip}}{1 + \mu_{tip}} \tag{14}$$

It can be clearly seen is that the center of gravity of the total blade is dependent only on the ratio of the tip and blade masses.
By experiment, the center of gravity of the blade was found to be located at 0.74 m from the root. By using this location, the mass ratio was calculated. The final values obtained from the above expressions are shown in Table 1.

## 2.4 Mass Moment of Inertia

The mass moment of inertia of the total blade, about the flapping axis at the root, can be calculated as per the following method.

$$J_{total} = \int_0^L r^2 dm_{blade} + m_{tip}L^2 \tag{15}$$

| Parameter | Value |
|---|---|
| $R$ | $2.0m$ |
| $L$ | $1.725m$ |
| $e$ | $0.1375$ |
| $c_0$ | $0.129m$ |
| $c_1$ | $-0.109m$ |
| $t_0$ | $0.0260m$ |
| $t_1$ | $-0.0253m$ |
| $\mu$ | $0.208$ |
| $m_{total}$ | $1.17kg$ |
| $m_{blade}$ | $0.969kg$ |
| $m_{tip}$ | $0.201kg$ |

Table 1: Calculated Parameters for Rotor Blade

The integral in the above expression is obtained as:

$$\int_0^L r^2 dV_{blade} = f_{airfoil} R^3 \int_0^{1-e} \bar{r}^2 (c_0 + c_1\bar{r}).(t_0 + t_1\bar{r}).d\bar{r}$$

$$= f_{airfoil} R^3 \int_0^{1-e} [c_0 t_0 \bar{r}^2 + (c_1 t_0 + c_0 t_1)\bar{r}^3 + c_1 t_1 \bar{r}^4].d\bar{r}$$

$$\int_0^L r^2.dV_{blade} = f_{airfoil} R^3 \left[ c_0 t_0 \frac{(1-e)^3}{3} + (c_1 t_0 + c_0 t_1)\frac{(1-e)^4}{4} + c_1 t_1 \frac{(1-e)^5}{5} \right] \tag{16}$$

The shape factor and blade density can be eliminated by using the expressions in Equations 5 and 8:

$$\rho_{blade} \int_0^L r^2 dV_{blade} = \rho_{blade} f_{airfoil} R^3 \left[ c_0 t_0 \frac{(1-e)^3}{3} + (c_1 t_0 + c_0 t_1)\frac{(1-e)^4}{4} + c_1 t_1 \frac{(1-e)^5}{5} \right]$$

$$= m_{blade} R^2 (1-e)^2 \left[ \frac{\frac{c_0 t_0}{3} + (c_1 t_0 + c_0 t_1)\frac{(1-e)}{4} + c_1 t_1 \frac{(1-e)^2}{5}}{c_0 t_0 + (c_1 t_0 + c_0 t_1)\frac{(1-e)}{2} + c_1 t_1 \frac{(1-e)^2}{3}} \right] \tag{17}$$

The inertia of the blade calculated from these equations is given in Table 2.

| | |
|---|---|
| $J_{blade}$ | $0.437 kg.m^2$ |
| $J_{total}$ | $1.036 kg.m^2$ |

Table 2: Inertia Calculation

| | |
|---|---|
| $EI_1/EI_0$ | $-3.762$ |
| $EI_2/EI_0$ | 5.301 |
| $EI_3/EI_0$ | $-3.316$ |
| $EI_4/EI_0$ | 0.7768 |

Table 3: Bending stiffness coefficient ratios

### 2.5 Area Moment of Inertia

For estimating the elasticity of the rotor blade in flap, the area moment of inertia of each cross-section becomes very important. The cross-sectional area moment of inertia is assumed to be proportional to the product of the area and the square of the blade thickness. The proportional constant is called $g_{airfoil}$. Hence,

$$I = g_{airfoil}(f_{airfoil}ct).t^2 \tag{18}$$

The bending stiffness is known as $EI$, of which we assume the elastic constant $E$ is uniform for the entire blade. This gives us the bending stiffness as a function of the radial location:

$$\begin{aligned} EI &= Eg_{airfoil}f_{airfoil}(c_0 + c_1\bar{r})(t_0 + t_1\bar{r})^3 \\ &= Eg_{airfoil}f_{airfoil}[c_0t_0^3 + (c_1t_0^3 + 3c_0t_1t_0^2)\bar{r} + (3c_0t_0t_1^2 + 3c_1t_1t_0^2)\bar{r}^2 + (c_0t_1^3 + 3c_1t_0t_1^2)\bar{r}^3 + c_1t_1^3\bar{r}^4] \\ &= EI_0 + EI_1\bar{r} + EI_2\bar{r}^2 + EI_3\bar{r}^3 + EI_4\bar{r}^4 \\ &= EI_0\left[1 + \left(\frac{c_1}{c_0} + \frac{3t_1}{t_0}\right)\bar{r} + 3\left(\frac{t_1^2}{t_0^2} + \frac{c_1t_1}{c_0t_0}\right)\bar{r}^2 + \left(\frac{t_1^3}{t_0^3} + 3\frac{c_1t_1^2}{c_0t_0^2}\right)\bar{r}^3 + \left(\frac{c_1t_1^3}{c_0t_0^3}\right)\bar{r}^4\right] \end{aligned} \tag{19}$$

It can be clearly seen that the bending stiffness is a fourth order polynomial in the radial location $\bar{r}$. It is proportional to a single parameter $EI_0$, while the rest of the coefficients can be easily calculated from the geometric parameters of thickness and chord length. The ratios of the different coefficients is given in Table 3.

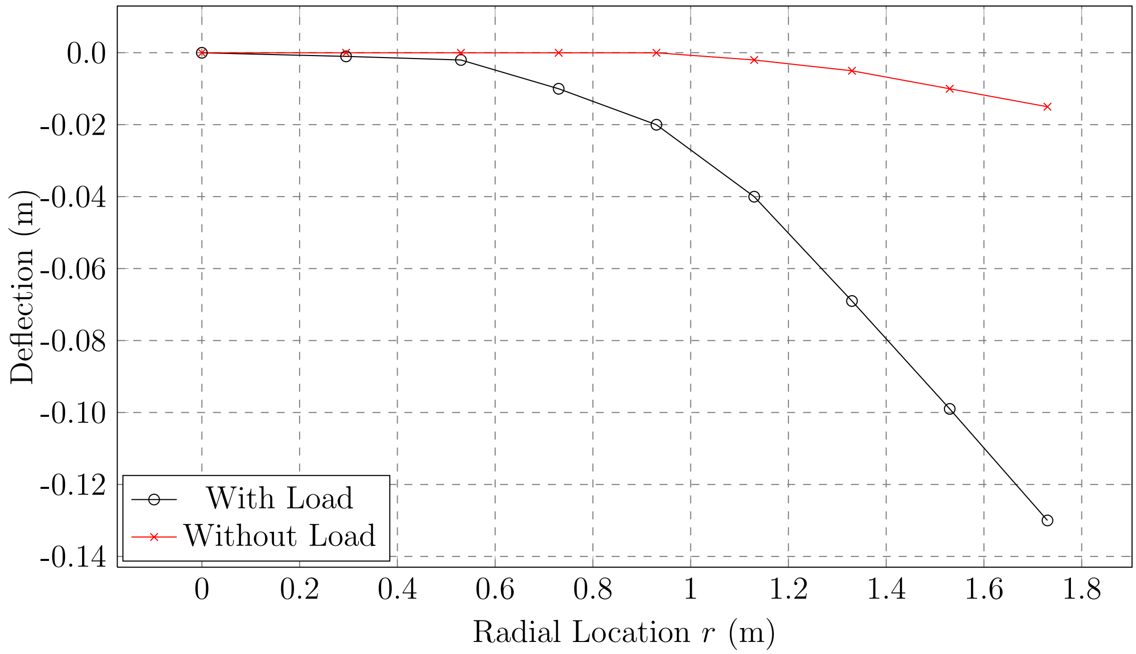


Figure 3: Blade Deflection Experiment

# 3 Finite Element Analysis

A simple finite element model for the blade was made based on the previous chapter. The Euler-Bernoulli beam bending theory was applied in this model.

## 3.1 Experiment

An experiment was conducted on the blade to estimate the blade stiffness, and validate the finite element model. In the first part of the experiment, the blade was fixed at the root and deflections due to the blade weight at various locations were measured. In the second set of experiment, the blade was loaded with weights and the resulting deflections were measured. The results of the experiment are plotted in Fig. 3. The blade loading is given in Table 4.

## 3.2 Formulation

The Euler-Bernoulli theory for beam bending tells us:

$$\frac{d^2}{dx^2}\left(EI\frac{d^2w}{dx^2}\right) = q \tag{20}$$

| **Section** | **Radial Location** r (m) | **Load** (kg) |
|---|---|---|
| 1 | 0.295 | 0.465 |
| 2 | 0.53 | 0.545 |
| 3 | 0.73 | 0.6 |
| 4 | 0.93 | 0.9 |
| 5 | 1.13 | 0.785 |
| 6 | 1.33 | 0.735 |
| 7 | 1.53 | 0.655 |
| 8 | 1.73 | 0.32 |

Table 4: Blade Loading

Where, $EI$ is the stiffness at the location $x$ from the root, and $w$ is the deflection due to the load $q$. We use a test function $u$ and integrating by parts:

$$\int_0^L EI\frac{d^2u}{dx^2}\frac{d^2w}{dx^2}dx = \int_0^L qwdx + \left[\left(EI\frac{d^2w}{dx^2}\right)\frac{du}{dx}\right]_0^L - \left[\frac{d}{dx}\left(EI\frac{d^2w}{dx^2}\right)u\right]_0^L \tag{21}$$

Now we assume the deflection to be a summation of basis functions $\phi_i$, with coefficients $\alpha_i$:

$$w_{FE} = \sum_{i=1}^{2N+2} \alpha_i\phi_i(x) \tag{22}$$

The test function is assigned as a basis function also:

$$u = \phi_j(x) \tag{23}$$

The choice of basis functions is such that they are double differentiable, which means they must be at least cubic polynomials. The normalized polynomials chosen are:

$$\hat{\phi}_1(\xi) = \frac{3}{4}(\xi-1)^2 + \frac{1}{4}(\xi-1)^3 \tag{24}$$

$$\hat{\phi}_2(\xi) = \frac{1}{2}(\xi-1)^2 + \frac{1}{4}(\xi-1)^3 \tag{25}$$

$$\hat{\phi}_3(\xi) = \frac{3}{4}(\xi+1)^2 - \frac{1}{4}(\xi+1)^3 \tag{26}$$

$$\hat{\phi}_4(\xi) = -\frac{1}{2}(\xi+1)^2 + \frac{1}{4}(\xi+1)^3 \tag{27}$$

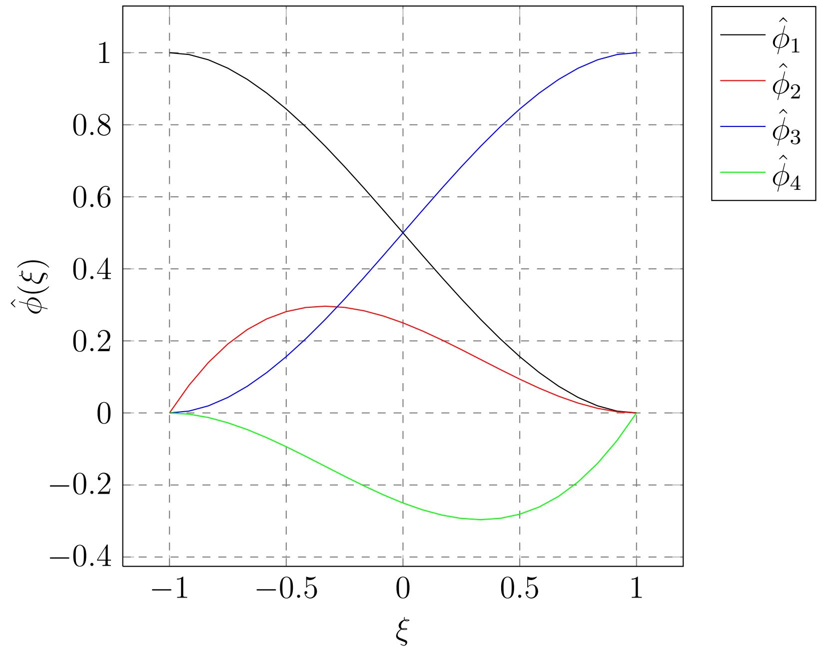


Figure 4: Basis Functions

Where $\xi$ lies between $-1$ to 1 in each element, with the endpoints as the nodes. The basis functions can be visualized in Fig. 4.

The blade was divided into 9 elements based on the nodes on which the loads were applied.

$$\sum_{i=0}^{N} \alpha_i \int_0^L EI \frac{d^2\phi_j}{dx^2} \frac{d^2\phi_i}{dx^2} dx = \sum_{i=0}^{N} \alpha_i \int_0^L q\phi_i dx + \sum_{i=0}^{N} \alpha_i \left[ \left( EI \frac{d^2\phi_i}{dx^2} \right) \frac{d\phi_j}{dx} \right]_0^L - \sum_{i=0}^{N} \alpha_i \left[ \frac{d}{dx} \left( EI \frac{d^2\phi_i}{dx^2} \right) \phi_j \right]_0^L \tag{28}$$

For each element, the following stiffness matrix was formed:

$$[k]^i_{4\times4} \Rightarrow k^i_{lm} = \int_{I_i} EI(\xi, i) \frac{d^2\hat{\phi}_l}{d\xi^2} \frac{d^2\hat{\phi}_m}{d\xi^2} \left( \frac{2}{L_i} \right)^3 d\xi \tag{29}$$

Where $L_i$ is the length of the $i^{th}$ element. Similarly the load matrix was formed:

$$[f]^i_{4\times1} \Rightarrow f^i_l = \int_{I_i} q(\xi, i) \hat{\phi}_l \left( \frac{L_i}{2} \right) d\xi \tag{30}$$

The integrals of the above are calculated using the Gauss-Legendre quadrature. The integral

| **Order** | **Roots** $\xi_i$ | **Weights** $W(\xi_i)$ | **Example** |
|---|---|---|---|
| 0 | 0 | 2 | $\int_{-1}^{1} a_0 d\xi = 2a_0 = 2.f(0)$ |
| 1 | 0 | 2 | $\int_{-1}^{1}(a_0 + a_1\xi)d\xi = 2a_0 = 2(a_0 + a_1.0) = 2.f(0)$ |
| 2 | $-\frac{1}{\sqrt{3}}, \frac{1}{\sqrt{3}}$ | 1,1 | $\int_{-1}^{1}(a_0 + a_1\xi + a_2\xi^2)d\xi = 2a_0 + 2a_2/3$ <br> $= 1.(a_0 + a_1/\sqrt{3} + a_2/3) + 1.(a_0 - a_1/\sqrt{3} + a_2/3)$ <br> $= 1.f(-1/\sqrt{3}) + 1.f(1/\sqrt{3})$ |
| 3 | $-\frac{1}{\sqrt{3}}, \frac{1}{\sqrt{3}}$ | 1,1 | $\int_{-1}^{1}(a_0 + a_1\xi + a_2\xi^2 + a_3\xi^3)d\xi = 2a_0 + 2a_2/3$ <br> $= 1.(a_0 + a_1/\sqrt{3} + a_2/3 + a_3/\sqrt{27})$ <br> $+1.(a_0 - a_1/\sqrt{3} + a_2/3 - a_3/\sqrt{27})$ <br> $= 1.f(-1/\sqrt{3}) + 1.f(1/\sqrt{3})$ |

Table 5: Gauss Legendre Integration

of a polynomial function over a given domain is equal to the sum of the product Gauss-Legendre weights with the value of the function at the roots.

$$\int f(r)dr = \sum_{i=1}^{n} f(\xi_i) * W_i \tag{31}$$

The mapping of the local $\xi$ to the global radial location $x$ is:

$$x(\xi, i) = \sum_{k=1}^{i-1} l(i) + (1+\xi)\frac{L_i}{2} \tag{32}$$

The element matrices were then combined to form the global stiffness and load matrices.

$$K(J, L) = K(J, L) + k_{jl}^{i} \tag{33}$$

$$F(J) = F(J) + f_j^i \tag{34}$$

We are then left with the following system:

$$[K]_{(2N+2)\times(2N+2)}\{\alpha\}_{(2N+2)\times 1} = [F]_{(2N+2)\times 1} \tag{35}$$

The boundary conditions are imposed appropriately in the load matrix and the system is

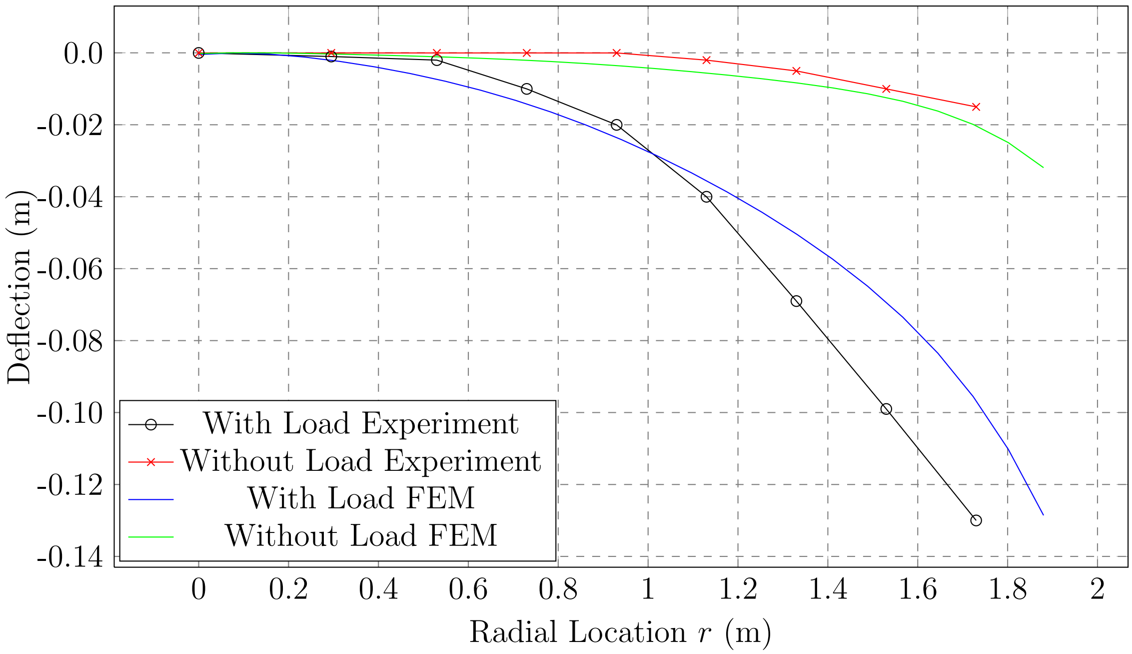


Figure 5: Blade Deflection Simulation

solved to obtain the coefficients $\alpha$. The unknown parameter in this simulation is the stiffness parameter $EI_0$. By varying its value, the deflections were matched with the experimental results. It was found that $EI_0 = 2200$ gave good results as shown in Fig. 5.
First the deflections from the two experiments were fit with a linear curve. This gave us:

- Without Load: $w(r) = 0.00787 * r - 0.00362$
- With Load: $w(r) = 0.0759 * r - 0.028$

The flap deflection is obtained from the slope of the line, by taking the inverse tangent:

- Without Load: $\beta = 0.0078698 rad$
- With Load: $\beta = 0.07575 rad$

For both the conditions, a virtual offset can be assumed where the blade has zero deflection. These two values turn out to be:

- Without Load: $e^* = 0.460m$
- With Load: $e^* = 0.369m$

The net moments at the virtual offset location comes out to be:

- Without Load: $M = 3.5374Nm$
- With Load: $M = 32.1231Nm$

The estimate of the spring constant is then obtained from:

$$K_\beta = \frac{M}{\beta} \tag{36}$$

- Without Load: $K_\beta = 449.5Nm/rad$
- With Load: $K_\beta = 424.0Nm/rad$

# 4 Rotor Aerodynamics

The coordinate systems were defined as shown in Fig. 6 The hub fixed coordinate system of the upper rotor is $\{X_u, Y_u, Z_u\}$. The transformation of the blade azimuth location at $\psi$ to $\{X'_u, Y'_u, Z'_u\}$ is:

$$\begin{bmatrix} X'_u \\ Y'_u \\ Z'_u \end{bmatrix} = \begin{bmatrix} \cos\psi & \sin\psi & 0 \\ -\sin\psi & \cos\psi & 0 \\ 0 & 0 & 1 \end{bmatrix} \times \begin{bmatrix} X_u \\ Y_u \\ Z_u \end{bmatrix} \tag{37}$$

The transformation of the blade flapping upwards with an angle $\beta$ to $\{X''_u, Y''_u, Z''_u\}$ is:

$$\begin{bmatrix} X''_u \\ Y''_u \\ Z''_u \end{bmatrix} = \begin{bmatrix} \cos\beta & 0 & \sin\beta \\ 0 & 1 & 0 \\ -\sin\beta & 0 & \cos\beta \end{bmatrix} \times \begin{bmatrix} X'_u \\ Y'_u \\ Z'_u \end{bmatrix} \tag{38}$$

This gives the overall transformation as:

$$\begin{bmatrix} X_u \\ Y_u \\ Z_u \end{bmatrix} = \begin{bmatrix} \cos\beta\cos\psi & -\sin\psi & \sin\beta\cos\psi \\ \cos\beta\sin\psi & \cos\psi & \sin\beta\sin\psi \\ -\sin\beta & 0 & \cos\beta \end{bmatrix} \times \begin{bmatrix} X''_u \\ Y''_u \\ Z''_u \end{bmatrix} \tag{39}$$

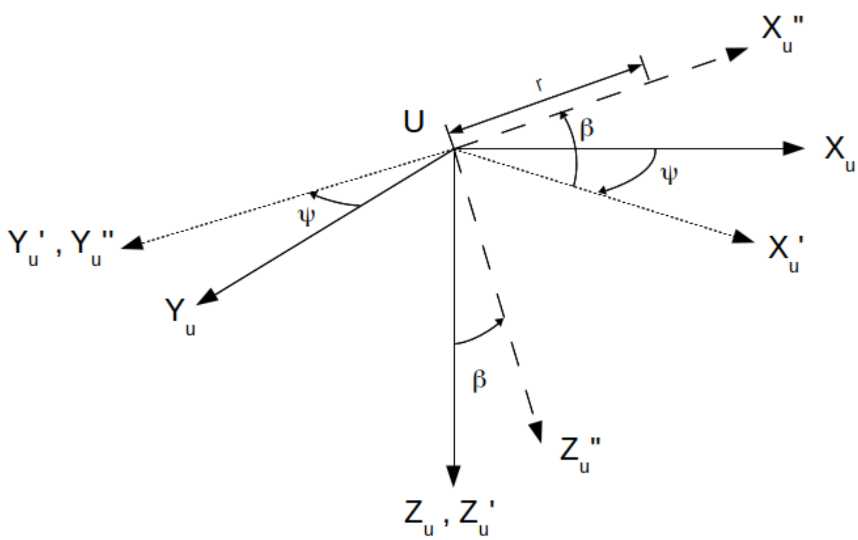


Figure 6: Rotor Coordinate Systems

## 4.1 Forward Flight

Assuming that the blade rotates clockwise, the angular velocity of a blade element is:

$$\vec{\omega} = \Omega\hat{Z} + \dot{\beta}\hat{Y}' = -\Omega\sin\beta\hat{X}'' + \dot{\beta}Y'' + \Omega\cos\beta\hat{Z}'' \tag{40}$$

If the offset is not considered, the position vector of the element is:

$$\vec{r} = r\hat{X}'' \tag{41}$$

This gives us the velocity as:

$$\vec{v} = \vec{\omega} \times \vec{r} = r\Omega\cos\beta\hat{Y}'' - r\dot{\beta}\hat{Z}'' \tag{42}$$

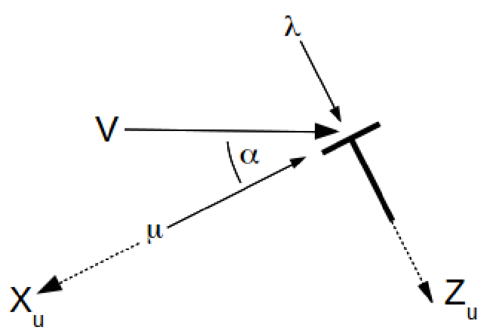


Figure 7: Hub Motion

The hub velocity can be divided into two components as shown in Fig. 7:

$$\mu = \frac{V\cos\alpha}{\Omega R} \tag{43}$$

$$\lambda = \frac{V\sin\alpha + v_i}{\Omega R} \tag{44}$$

which gives us the speed of the air:

$$\vec{v}_{air} = -\mu\Omega R\hat{X} + \lambda\Omega R\hat{Z} \tag{45}$$

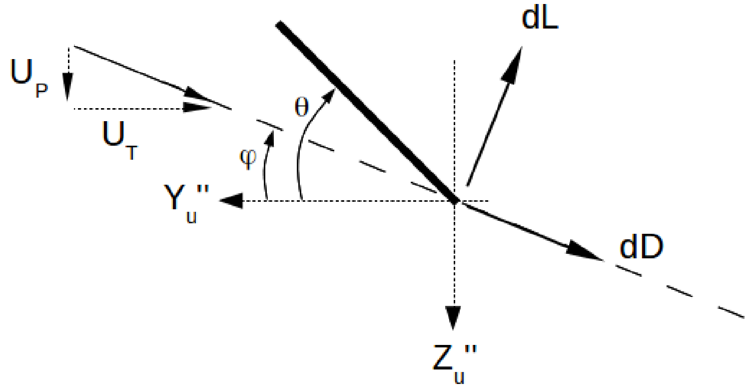


Figure 8: Blade Element

The relative velocity of Air over the blade becomes:

$$\vec{v_{rel}} = \vec{v_{air}} - \vec{v}$$
$$= -\Omega R(\mu \cos\psi \cos\beta + \lambda \sin\beta)\hat{X}''$$
$$+\Omega R(\mu \sin\psi - \bar{r}\cos\beta)\hat{Y}''$$
$$+\Omega R(\lambda \cos\beta - \mu \cos\psi \sin\beta + \bar{r}\beta^*)\hat{Z}''$$

The approximation is made that

$$\beta \to 0 \qquad \Rightarrow \qquad \cos\beta \approx 1 \qquad , \qquad \sin\beta \approx \beta$$

The relative perpendicular and tangential components of air with respect to blade become:

$$\bar{U}_P = \frac{U_P}{\Omega R} = \lambda - \mu\beta\cos\psi + \bar{r}\beta^* \tag{46}$$

$$\bar{U}_T = \frac{U_T}{\Omega R} = \bar{r} - \mu \sin\psi \tag{47}$$

The forces on each blade element can be seen in Fig. 8. The lift and drag are approximated to the following:

$$dL = \frac{1}{2}\rho U_T^2 ca(\theta - \phi) \tag{48}$$

$$dD = \frac{1}{2}\rho U_T^2 cC_{Do} \tag{49}$$

$$\begin{bmatrix} dF_{X''} \\ dF_{Y''} \\ dF_{Z''} \end{bmatrix} = \begin{bmatrix} 0 \\ -dL\sin\phi - dD\cos\phi \\ dD\sin\phi - dL\cos\phi \end{bmatrix} = \begin{bmatrix} 0 \\ -\phi dL - dD \\ \phi dD - dL \end{bmatrix} \tag{50}$$

$$\begin{bmatrix} dF_{X} \\ dF_{Y} \\ dF_{Z} \end{bmatrix} = \begin{bmatrix} \cos\psi & -\sin\psi & \beta\cos\psi \\ \beta\sin\psi & \cos\psi & \beta\sin\psi \\ -\beta & 0 & 1 \end{bmatrix} \times \begin{bmatrix} 0 \\ -\phi dL - dD \\ -dL \end{bmatrix} \tag{51}$$

$$d\vec{M} = \vec{r} \times d\vec{F} \tag{52}$$

$$\begin{bmatrix} dM_{X} \\ dM_{Y} \\ dM_{Z} \end{bmatrix} = \begin{bmatrix} 0 \\ -rdF_{Z''} \\ rdF_{Y''} \end{bmatrix} \tag{53}$$

$$\begin{bmatrix} dM_{X''} \\ dM_{Y''} \\ dM_{Z''} \end{bmatrix} = \begin{bmatrix} \cos\psi & -\sin\psi & \beta\cos\psi \\ \beta\sin\psi & \cos\psi & \beta\sin\psi \\ -\beta & 0 & 1 \end{bmatrix} \times \begin{bmatrix} 0 \\ -rdF_{Z''} \\ rdF_{Y''} \end{bmatrix} \tag{54}$$

### 4.1.1 Assumptions in Geometry

We assume a linear taper and twist in the blade:

$$c = c_0 + c_1\bar{r} \tag{55}$$

$$\theta = \theta_0 + \theta_1\bar{r} \tag{56}$$

The rotor flap is assumed to be as the first harmonic in the rotor revolutions:

$$\beta = \beta_0 + \beta_{1c}\cos\psi + \beta_{1s}\sin\psi \tag{57}$$

$$\dot{\beta} = \Omega(\beta_{1s}\cos\psi - \beta_{1c}\sin\psi) \tag{58}$$

The derivatives are normalized with the rotation speed of the rotor:

$$\beta^{*} = \beta_{1s}\cos\psi - \beta_{1c}\sin\psi \tag{59}$$

$$\beta^{**} = -\beta_{1c}\cos\psi - \beta_{1s}\sin\psi \tag{60}$$

#### 4.1.2 Forces

The rotor forces are averaged over one revolution to obtain:

$$\begin{aligned}
F_X = &\left(\frac{N\rho\Omega^2R^3ac_0}{2}\right)\left[\frac{3\lambda\beta_{1c}}{4}+\frac{\beta_0\beta_{1c}}{6}-\frac{\mu}{4}\left(\beta_0^2+\beta_{1c}^2\right)+\theta_0\left(\frac{\mu\lambda}{2}-\frac{\beta_{1c}}{3}\right)+\theta_1\left(\frac{\mu\lambda}{4}-\frac{\beta_{1c}}{4}\right)\right]\\
&+\left(\frac{N\rho\Omega^2R^3ac_1}{2}\right)\left[\frac{\lambda\beta_{1c}}{2}+\frac{\beta_0\beta_{1c}}{8}-\frac{\mu}{6}\left(\beta_0^2+\beta_{1c}^2\right)+\theta_0\left(\frac{\mu\lambda}{4}-\frac{\beta_{1c}}{4}\right)+\theta_1\left(\frac{\mu\lambda}{6}-\frac{\beta_{1c}}{5}\right)\right]\\
&-\left(\frac{N\rho\Omega^2R^3C_{Do}\mu}{2}\right)\left[\frac{c_0}{2}+\frac{c_1}{3}\right]
\end{aligned} \tag{61}$$

$$\begin{aligned}
F_Y = &\left(\frac{N\rho\Omega^2R^3ac_0}{2}\right)\\
&\left[\frac{3\lambda\beta_{1s}}{4}-\frac{3\lambda\mu\beta_0}{2}+\mu^2\beta_0\beta_{1c}-\frac{\beta_0\beta_{1c}}{6}-\frac{\mu\beta_{1c}\beta_{1s}}{4}+\theta_0\left(\frac{3\mu\beta_0}{4}-\frac{\beta_{1s}}{3}-\frac{\mu^2\beta_{1s}}{2}\right)+\theta_1\left(\frac{\mu\beta_0}{2}-\frac{\beta_{1s}}{4}-\frac{\mu^2\beta_{1s}}{4}\right)\right]\\
&+\left(\frac{N\rho\Omega^2R^3ac_1}{2}\right)\\
&\left[\frac{\lambda\beta_{1s}}{2}-\frac{3\lambda\mu\beta_0}{4}+\frac{\mu^2\beta_0\beta_{1c}}{2}-\frac{\beta_0\beta_{1c}}{8}-\frac{\mu\beta_{1c}\beta_{1s}}{6}+\theta_0\left(\frac{\mu\beta_0}{2}-\frac{\beta_{1s}}{4}-\frac{\mu^2\beta_{1s}}{4}\right)+\theta_1\left(\frac{3\mu\beta_0}{8}-\frac{\beta_{1s}}{5}-\frac{\mu^2\beta_{1s}}{6}\right)\right]
\end{aligned} \tag{62}$$

$$\begin{aligned}
F_Z = &-\left(\frac{N\rho\Omega^2R^3ac_0}{2}\right)\left[\theta_0\left(\frac{1}{3}+\frac{\mu^2}{2}\right)+\theta_1\left(\frac{1}{4}+\frac{\mu^2}{4}\right)-\frac{\lambda}{2}\right]\\
&-\left(\frac{N\rho\Omega^2R^3ac_1}{2}\right)\left[\theta_0\left(\frac{1}{4}+\frac{\mu^2}{4}\right)+\theta_1\left(\frac{1}{5}+\frac{\mu^2}{6}\right)-\frac{\lambda}{3}\right]
\end{aligned} \tag{63}$$

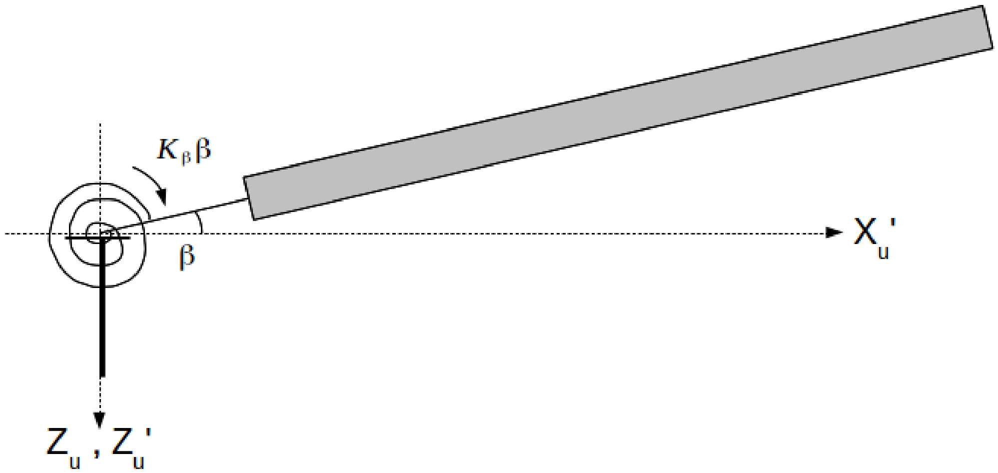


Figure 9: Rotor Flapping Model

### 4.1.3 Moments

$$M_X = -\frac{NK_\beta \beta_{1s}}{2} \tag{64}$$

$$M_Y = \frac{NK_\beta \beta_{1c}}{2} \tag{65}$$

$$\begin{aligned} M_Z = &\left(\frac{N\rho\Omega^2 R^4 c_0}{2}\right) \times \\ &\left[a\left(\frac{\lambda^2}{2} - \frac{\lambda\mu\beta_{1c}}{2} + \frac{\mu^2\beta_0^2}{4} - \frac{\mu\beta_{1s}\beta_0}{3} + \frac{\beta_{1c}^2}{8} + \frac{\beta_{1s}^2}{8} + \frac{3\mu^2\beta_{1c}^2}{16} + \frac{\mu^2\beta_{1s}^2}{16} - \frac{\theta_0\lambda}{3} - \frac{\theta_1\lambda}{4}\right) - C_{D_o}\left(\frac{1}{4} + \frac{\mu^2}{4}\right)\right] \\ &+ \left(\frac{N\rho\Omega^2 R^4 c_1}{2}\right) \times \\ &\left[a\left(\frac{\lambda^2}{3} - \frac{\lambda\mu\beta_{1c}}{3} + \frac{\mu^2\beta_0^2}{6} - \frac{\mu\beta_{1s}\beta_0}{4} + \frac{\beta_{1c}^2}{10} + \frac{\beta_{1s}^2}{10} + \frac{\mu^2\beta_{1c}^2}{8} + \frac{\mu^2\beta_{1s}^2}{24} - \frac{\theta_0\lambda}{4} - \frac{\theta_1\lambda}{5}\right) - C_{D_o}\left(\frac{1}{5} + \frac{\mu^2}{6}\right)\right] \end{aligned} \tag{66}$$

## 4.2 Rotor Flapping

The blade is assumed to be rigid with a root spring at the hub center to account for the flexibility of the blade. The blade flapping differential equation is formed, and solved for each of the terms in the flapping assumption.

$$\begin{aligned} &\beta^{**} + \frac{\rho a R^4}{2J_b}\left[c_0\left(\frac{1}{4} - \frac{\mu\sin\psi}{3}\right) + c_1\left(\frac{1}{5} - \frac{\mu\sin\psi}{4}\right)\right]\beta^* + \\ &\left[\bar{\omega}^2_{RF} - \frac{\rho a R^4 \mu\cos\psi}{2J_b}\left\{c_0\left(\frac{1}{3} - \frac{\mu\sin\psi}{2}\right) + c_1\left(\frac{1}{4} - \frac{\mu\sin\psi}{3}\right)\right\}\right]\beta \\ &= \frac{\rho a c_0 R^4}{2J_b}\left[\theta_0\left(\frac{1}{4} - \frac{2\mu\sin\psi}{3} + \frac{\mu^2\sin^2\psi}{2}\right) + \theta_1\left(\frac{1}{5} - \frac{\mu\sin\psi}{2} + \frac{\mu^2\sin^2\psi}{3}\right) - \frac{\lambda}{3} + \frac{\lambda\mu\sin\psi}{2}\right] \\ &+ \frac{\rho a c_1 R^4}{2J_b}\left[\theta_0\left(\frac{1}{5} - \frac{\mu\sin\psi}{2} + \frac{\mu^2\sin^2\psi}{3}\right) + \theta_1\left(\frac{1}{6} - \frac{2\mu\sin\psi}{5} + \frac{\mu^2\sin^2\psi}{4}\right) - \frac{\lambda}{4} + \frac{\lambda\mu\sin\psi}{3}\right] \end{aligned} \tag{67}$$

This gives us the following:

$$\beta_0 = \frac{\rho a R^4}{2J_b\bar{\omega}^2_{RF}}\left[c_0\left\{\theta_0\left(\frac{1}{4} + \frac{\mu^2}{4}\right) + \theta_1\left(\frac{1}{5} + \frac{\mu^2}{6}\right) - \frac{\lambda}{3}\right\} + c_1\left\{\theta_0\left(\frac{1}{5} + \frac{\mu^2}{6}\right) + \theta_1\left(\frac{1}{6} + \frac{\mu^2}{8}\right) - \frac{\lambda}{4}\right\}\right] \tag{68}$$

$$\beta_{1s} = \frac{Ak + B\bar{\omega}^2_{NRF}}{k^2 + \bar{\omega}^4_{NRF}} \tag{69}$$

$$\tag{70}$$

$$\beta_{1c} = \frac{A\bar{\omega}^2_{NRF} - Bk}{k^2 + \bar{\omega}^4_{NRF}} \tag{71}$$

Here:

$$\bar{\omega}^2_{NRF} = \frac{K_\beta}{J_b\Omega^2} \tag{72}$$

$$\bar{\omega}^2_{RF} = 1 + \bar{\omega}^2_{NRF} = 1 + \frac{K_\beta}{J_b\Omega^2} \tag{73}$$

$$A = \left(\frac{\rho a R^4 \mu}{2J_b}\right)\left[\frac{c_0}{3} + \frac{c_1}{4}\right]\beta_0 \tag{74}$$

$$B = \left(\frac{\rho a R^4 \mu}{2J_b}\right)\left[c_0\left(\frac{\lambda}{2} - \frac{2\theta_0}{3} - \frac{\theta_1}{2}\right) + c_1\left(\frac{\lambda}{3} - \frac{\theta_0}{2} - \frac{2\theta_1}{5}\right)\right] \tag{75}$$

$$k = \left(\frac{\rho a R^4}{2J_b}\right)\left[c_0\left(\frac{1}{4}-\frac{\mu^2}{8}\right)+c_1\left(\frac{1}{5}-\frac{\mu^2}{12}\right)\right] \tag{76}$$

The above forces and moments are for a clockwise rotating rotor (viewed from above). The forces for an anticlockwise rotating rotor can be found by simply taking the mirror image as shown in the following Fig. 10.

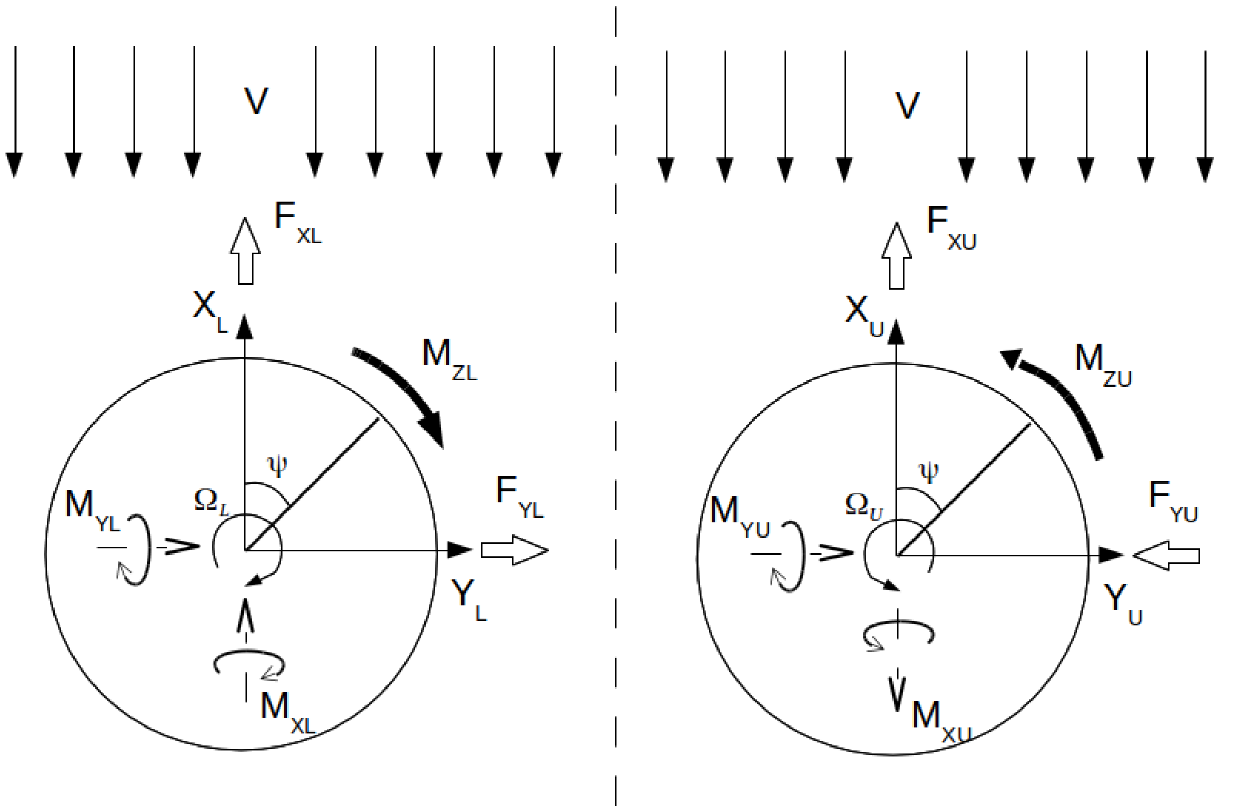


Figure 10: Mirror Image

Hence:

$$\begin{bmatrix} F_X \\ F_Y \\ F_Z \end{bmatrix}_{Counter-Clockwise} = \begin{bmatrix} F_X \\ -F_Y \\ F_Z \end{bmatrix}_{Clockwise} \tag{77}$$

$$\begin{bmatrix} M_X \\ M_Y \\ M_Z \end{bmatrix}_{Counter-Clockwise} = \begin{bmatrix} -M_X \\ M_Y \\ -M_Z \end{bmatrix}_{Clockwise} \tag{78}$$

## 4.3 Inflow Model

There are two models used in the report. The uniform inflow model is based on the momentum theory and is used in the closed form solution of the forces and moments used above. It also shows an accurate method to obtain the inflow, compared to the approximations used in the old analysis.

### 4.3.1 Uniform Inflow

The induced component of the inflow is obtained from momentum theory as the following:

$$\lambda_i = \frac{C_T}{2\sqrt{\mu^2 + (\lambda_c + \lambda_i)^2}} \tag{79}$$

$$\lambda = \lambda_c + \lambda_i \tag{80}$$

At hover we know that:

$$\lambda_h = (\lambda_i)_h = \sqrt{\frac{C_T}{2}} \tag{81}$$

Hence the induced inflow can be written in this form:

$$\lambda_i^* = \frac{1}{\sqrt{\mu^{*2} + (\lambda_c^* + \lambda_i^*)^2}} \tag{82}$$

Where:

$$\lambda_i^* = \frac{\lambda_i}{\lambda_h} \tag{83}$$

$$\mu^* = \frac{\mu}{\lambda_h} \tag{84}$$

$$\lambda_c^* = \frac{\lambda_c}{\lambda_h} \tag{85}$$

### 4.3.2 Newton's Method for solving $\lambda_i$

Let us define a function:

$$f(\lambda_i^*, \mu^*, \lambda_c^*) = \lambda_i^* - \frac{1}{\sqrt{\mu^{*2} + (\lambda_c^* + \lambda_i^*)^2}} \tag{86}$$

The partial derivative with respect to $\lambda_i^*$ is:

$$\frac{\partial f}{\partial \lambda_i^*} = 1 + \frac{\lambda_c^* + \lambda_i^*}{[\mu^{*2} + (\lambda_c^* + \lambda_i^*)^2]^{\frac{3}{2}}} \tag{87}$$

This function is zero when the $\lambda_i^*$ is converged. Using Newton's method, the consecutive values of $\lambda_i^*$ in each iteration can be obtained from the following:

$$(\lambda_i^*)_{n+1} = (\lambda_i^*)_n - \frac{f}{\left(\dfrac{\partial f}{\partial \lambda_i^*}\right)} \tag{88}$$

It was observed that since the function f is smooth and well behaved, the convergence of the solution came in just a few (3-4) iterations.

### 4.3.3 Drees Model

The Drees Model essentially assumes a non uniform distribution of inflow over the rotor in forward flight. The inflow calculated from the uniform inflow model is labeled as $\lambda_0$. The inflow at a particular radial location and azimuth is given as :

$$\lambda = \lambda_0 + \lambda_{1c}\bar{r}\cos\psi + \lambda_{1s}\bar{r}\sin\psi \tag{89}$$

The two components of the inflow distribution are given by:

$$\lambda_i = \lambda_0 - \lambda_c \tag{90}$$

$$\lambda_{1c} = \left(\frac{4}{3}\right)\lambda_i\left[\left(1 - \frac{9}{5}\mu^2\right)\sqrt{1 + \left(\frac{\lambda_i}{\mu}\right)^2} - \frac{\lambda_i}{\mu}\right] \tag{91}$$

$$\lambda_{1s} = 2\lambda_i\mu \tag{92}$$

### 4.3.4 Upper - Lower Rotor Interaction

The upper and lower rotor interaction is quantized by a factor K. This represents the speeding up of the upper rotor inflow which acts as a climb inflow to the lower rotor.

$$\lambda_{c,lower} = K\lambda_{0,upper}\frac{\Omega_U}{\Omega_L} \tag{93}$$

An analytic approximation of this interaction factor is dependent on the rotor spacing:

$$K = 1 + \frac{2H/D}{\sqrt{1 + 4H^2/D^2}} \quad (94)$$

For the current rotor spacing of $H = 0.19m$, and rotor diameter $D = 4.0m$, the interaction factor is found to be $K = 1.095$

## 4.4 Full Model

It is possible to numerically integrate the elemental loads without taking assumptions such as small flap angles into account. So in this case, for each azimuth location, the forces and moments are added as per the Gauss-Legendre integration scheme shown earlier. The steps followed are:

1. $\bar{r} = (1 - e)(1 + \xi_i)/2$
2. $c = c_0 + c_1\bar{r}$
3. $\theta = \theta_0 + \theta_1\bar{r}$
4. $\lambda = \lambda_0 + \lambda_{1c}\bar{r}\cos\psi + \lambda_{1s}\bar{r}\sin\psi$
5. $\bar{U}_T = -\mu_x \sin\psi + \mu_y \cos\psi + e + \bar{r}\cos\beta$
6. $\bar{U}_P = -\mu_y \sin\psi \sin\beta - \mu_x \cos\psi \sin\beta + \lambda\cos\beta + \beta^*(e\cos\beta + \bar{r})$
7. $\phi = tan^{-1}(\bar{U}_P/\bar{U}_T)$
8. $v = \Omega R(\bar{U}_T^2 + \bar{U}_P^2)$
9. $dL = (1/2)\rho v^2 ca(\theta - \phi)$
10. $dD = (1/2)\rho v^2 cC_{Do}$

The forces and moments are integrated using the Gauss-Legendre weights. The blade flapping differential equation is given by:

$$(J_b + M_b X_{cg} eR\cos\beta)\ddot{\beta} = M_{aerod} - K_\beta(\beta - \beta_{pre}) - (J_b + M_b X_{cg} eR\cos\beta)(\Omega^2 - \dot{\beta}^2)\sin\beta - J_b\dot{\beta}^2\cos\beta \quad (95)$$

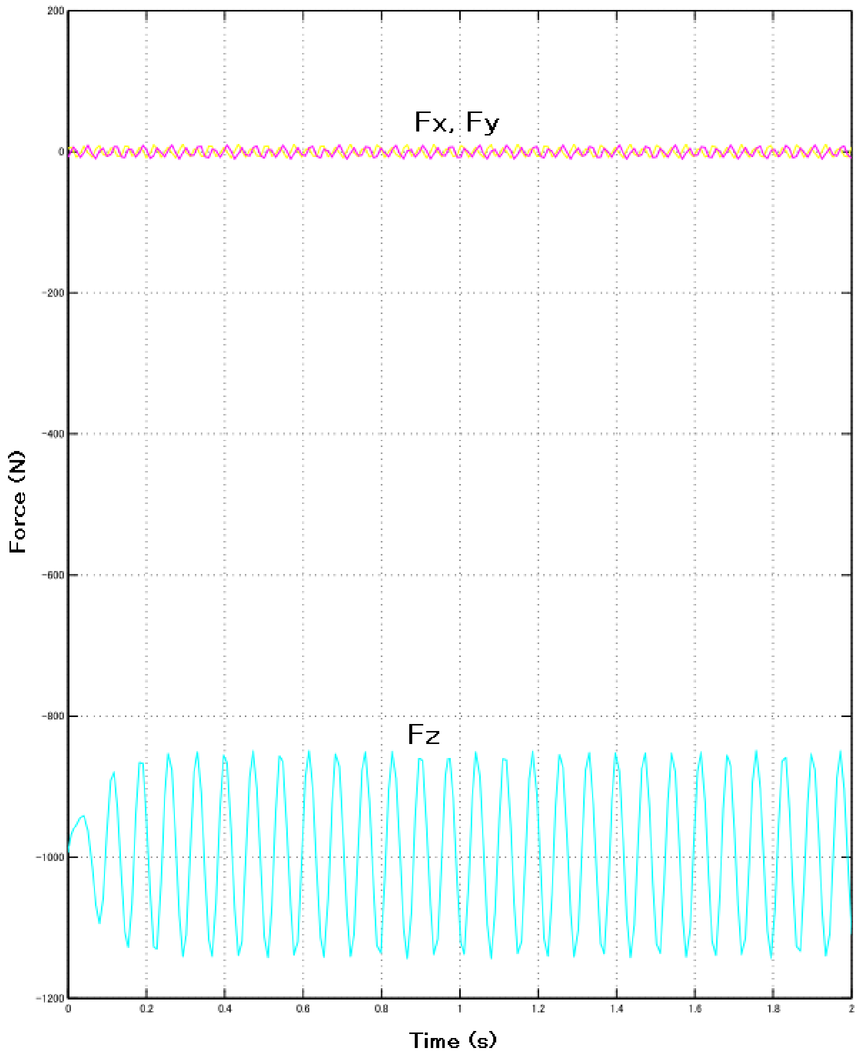


Figure 11: Upper Rotor Forces in forward flight of 5m/s

For example, the exact loads on the rotor can be seen in Fig. 11. The forces are calculated at a forward speed of 5m/s without any pitch tilt. It is clear that there is a large oscillatory load in the vertical direction at a frequency of nearly 14 Hz.

# 5 Forward Flight Equilibrium

The vehicle in forward flight and equilibrium is shown in Fig. 12.

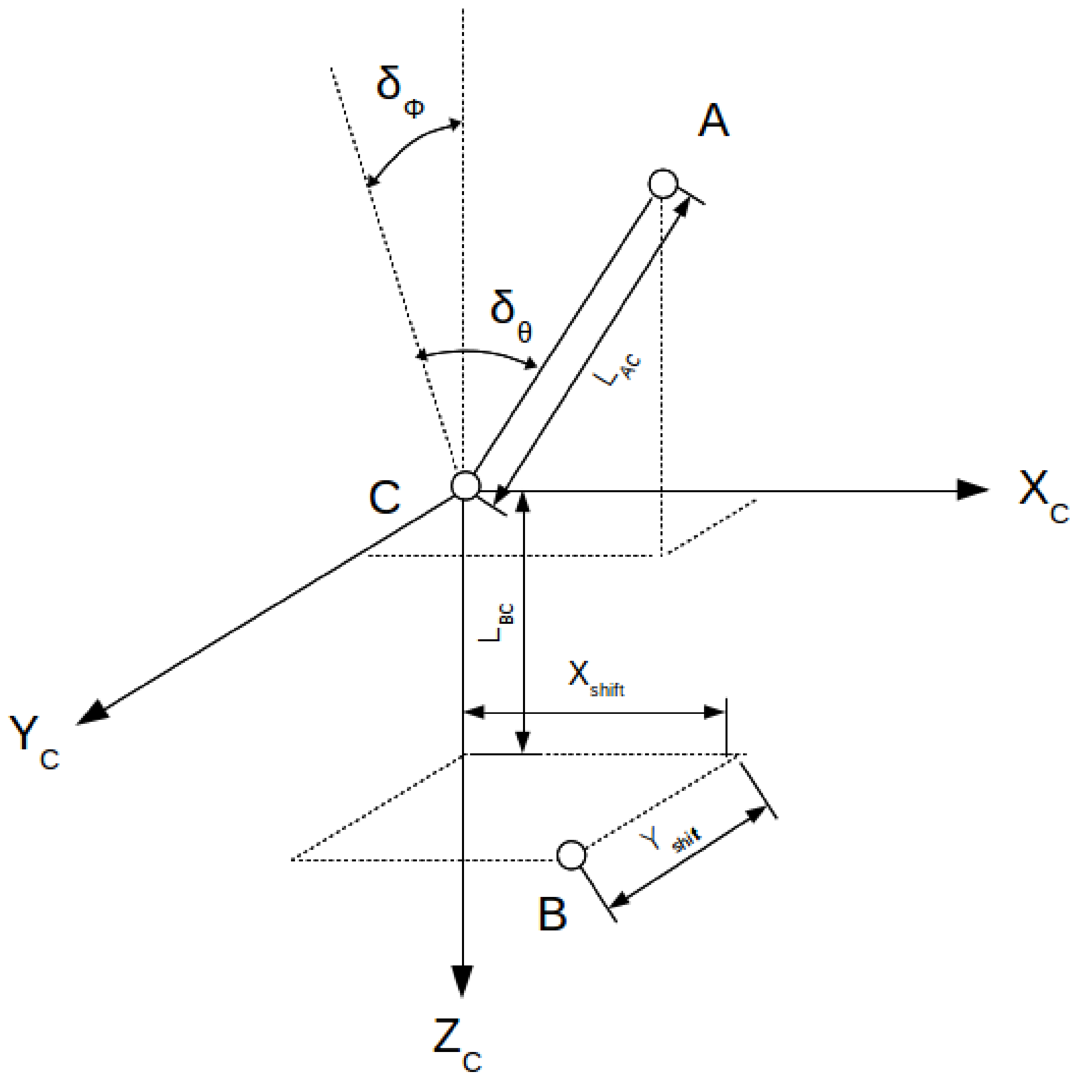


Figure 12: Forward Flight Model

The net mass of the upper and lower rotor is clumped with the mass of the mission unit at A. The point C is the universal joint about which the rotor shaft is allowed to tilt by $(\delta_\theta, \delta_\phi)$. The point B clumps the mass of the frame unit. It is assumed that the frame attached to C does not rotate with respect to the earth fixed coordinate system. This means that the payload in the frame does not have any different attitude during flight.

The CG location with respect to C can be obtained as:

$$X_{cg} = \frac{M_B X_{shift} + M_A L_{AC} \sin\delta_\theta}{M_A + M_B} \tag{96}$$

$$Y_{cg} = \frac{M_B Y_{shift} + M_A L_{AC} \cos\delta_\theta \sin\delta_\phi}{M_A + M_B} \tag{97}$$

$$Z_{cg} = \frac{M_B L_{BC} - M_A L_{AC} \cos\delta_\theta \cos\delta_\phi}{M_A + M_B} \tag{98}$$

## 5.1 Equilibrium

The coordinate transformation from the tilted A frame to the C frame is given by:

$$\begin{bmatrix} X_C \\ Y_C \\ Z_C \end{bmatrix} = \begin{bmatrix} \cos\delta_\theta & 0 & -\sin\delta_\theta \\ -\sin\delta_\theta \sin\delta_\phi & \cos\delta_\phi & -\cos\delta_\theta \sin\delta_\phi \\ \sin\delta_\theta \cos\delta_\phi & \sin\delta_\phi & \cos\delta_\theta \cos\delta_\phi \end{bmatrix} \times \begin{bmatrix} X_A \\ Y_A \\ Z_A \end{bmatrix} \tag{99}$$

The forces on the upper and lower rotor are clumped and transformed to the C frame for force balance. The other forces are from gravity and drag on the vehicle.

$$\begin{bmatrix} F_X \\ F_Y \\ F_Z \end{bmatrix}_C = \vec{F}_{Upper} + \vec{F}_{Lower} + \begin{bmatrix} 0 \\ 0 \\ (M_A + M_B)g \end{bmatrix}_C + \begin{bmatrix} -\frac{1}{2}\rho V^2 (\pi R^2)(f_A + f_B) \\ 0 \\ 0 \end{bmatrix}_C \tag{100}$$

Similarly, the net moment at the CG is calculated as:

$$\begin{bmatrix} M_X \\ M_Y \\ M_Z \end{bmatrix}_C = \vec{M}_{Upper} + \vec{M}_{Lower} + \vec{r}_{cg-U} \times \vec{F}_{Upper} + \vec{r}_{cg-L} \times \vec{F}_{Lower} + \vec{r}_{cg-A} \times \vec{F}_{Drag,A} + \vec{r}_{cg-B} \times \vec{F}_{Drag,B} \tag{101}$$

Equilibrium is that point at which the net force and moment at the center of gravity becomes zero.

## 5.2 Particle Swarm Optimization

We have six unknowns to solve for in the net force and moment equations. These unknowns are:

1. Upper Rotor Rotation speed: $\Omega_U$

2. Lower Rotor Rotation speed: $\Omega_L$

3. Forward Shift of Frame Unit: $X_{shift}$

4. Side-ward Shift of Frame Unit: $Y_{shift}$

5. Forward tilt of Mission Unit: $\delta_\theta$

6. Side-ward tilt of Mission Unit: $\delta_\phi$

At equilibrium, the net forces and moments are zero, so we define an objective function:

$$f = F_X^2 + F_Y^2 + F_Z^2 + M_X^2 + M_Y^2 + M_Z^2 \tag{102}$$

The unknown values become the parameters to optimize at a particular forward speed so that the objective function is minimized. For this we use the Particle Swarm Optimization technique.

## 5.3 Algorithm

The following algorithm is used to find the optimum values of the controls, given a forward velocity V:

1. Initialize 30 particles. The first particle is an initial user guess. The other particles are randomly given values in a given domain of about$\pm 10\%$ RPMs, $\pm 0.1 rad$ tilt and $\pm 0.1 m$ shifts.

2. Each particle is given its personal best optimum value as the calculated value of the optimum function at the given controls. A global best value is calculated by finding the minimum of them.

3. A tolerance of the optimum function is set to $10^{-10}$.

4. Then the personal and global best optimum function of the particles are found.

5. A velocity for each particle is found for each control as: $V_{n+1} = 0.5V_n + 2.Rand.(pbest - P_n) + 2.Rand.(gbest - P_n)$

6. The new position for each particle is found for each control as: $P_{n+1} = P_n + V_{n+1}$

7. This is repeated till the global best meets the tolerance required, and the global best particle is found to be optimum controls at equilibrium.

## 5.4 Results

The relation between the control inputs and the forward speed was plotted. The analysis of the results gives us an important indication of limits in forward speed.
An important limit is the region of reverse stall in the rotor. The region can be seen as the one with the darkest blue shade in the Fig.13. This region is seen to be a significant portion of the rotor at 10 m/s, especially in the lower rotor. The blade tilt and flap can also be seen in this figure.

The reverse stall region is approximately circular. At the points on the circumference, the tangential speed is zero. Hence, the diameter of this region is found by equating the forward speed and the speed due to rotation:

$$V = \Omega d \tag{103}$$

To keep this region as small as possible, it is important to have a high angular speed in forward flight. This can be achieved by reducing the pitch angle of the blades. However, this will increase the power requirement at hover.

The control inputs required at different forward speeds are plotted in Figs. 14-19. It can be seen that the rotor RPM decreases with forward speed. It does not significantly depend on the stiffness of the rotor blade, except at high speeds. Similarly, the forward tilt of the rotor is nearly independent of the stiffness of the blades. However, the sideways tilt is very dependent on the forward speed. In fact, for some mean values of the spring constant, the control reverses as speed increases. For flexible blades (K = 200), the tilt is roughly constant for speeds above 5m/s, implying that the control is easier. A very stiff blade will require large tilts. The forward shift in CG can be limited by using more flexible blades. The same conclusion is for the sideways shift.

The rotor power is not a limit to forward speed, since the maximum power is used at hover.

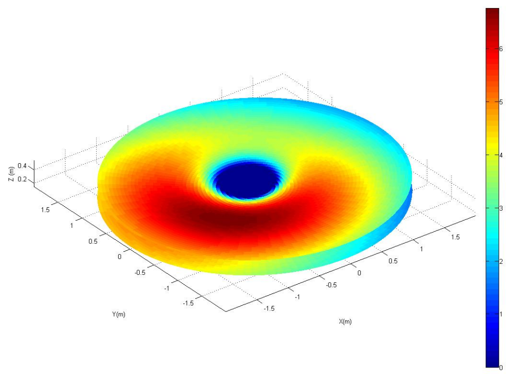


(a) Isometric View

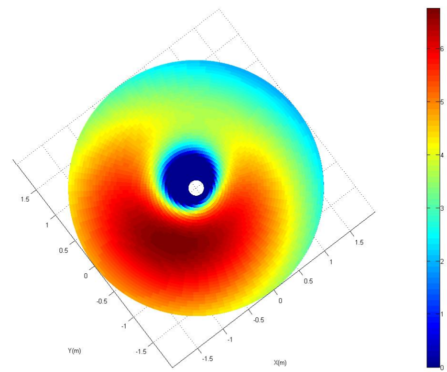


(b) Upper Rotor Top View

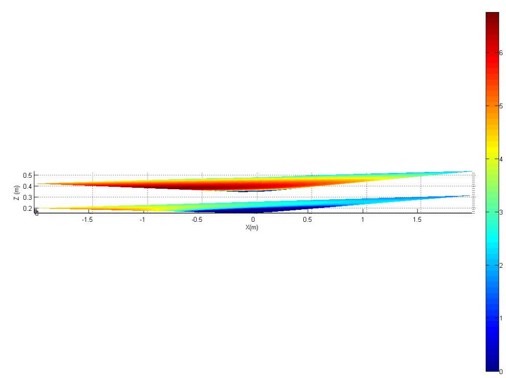


(c) Side View

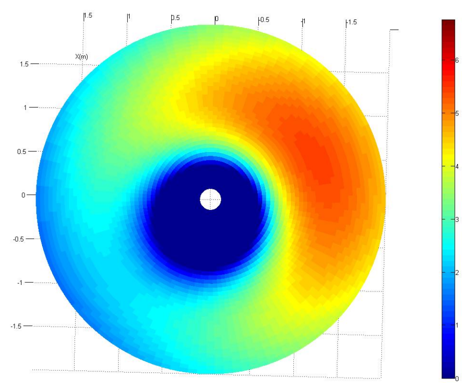


(d) Lower Rotor Bottom View

Figure 13: Rotor Angle of Attack at 10 m/s (36 km/hr) Forward Flight

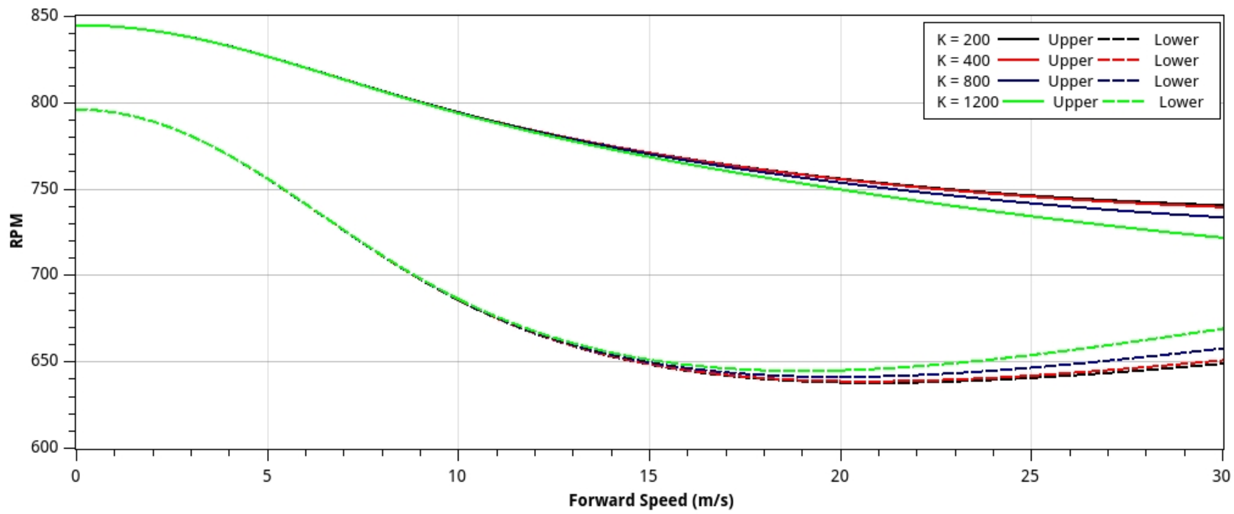


Figure 14: RPM variation in forward flight

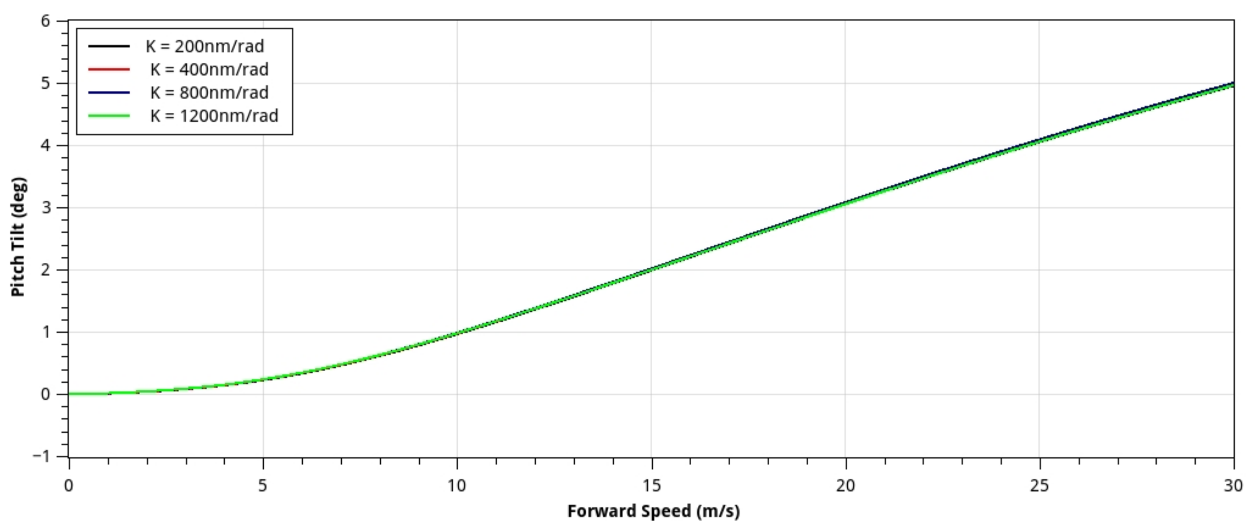


Figure 15: Pitch tilt variation in forward flight

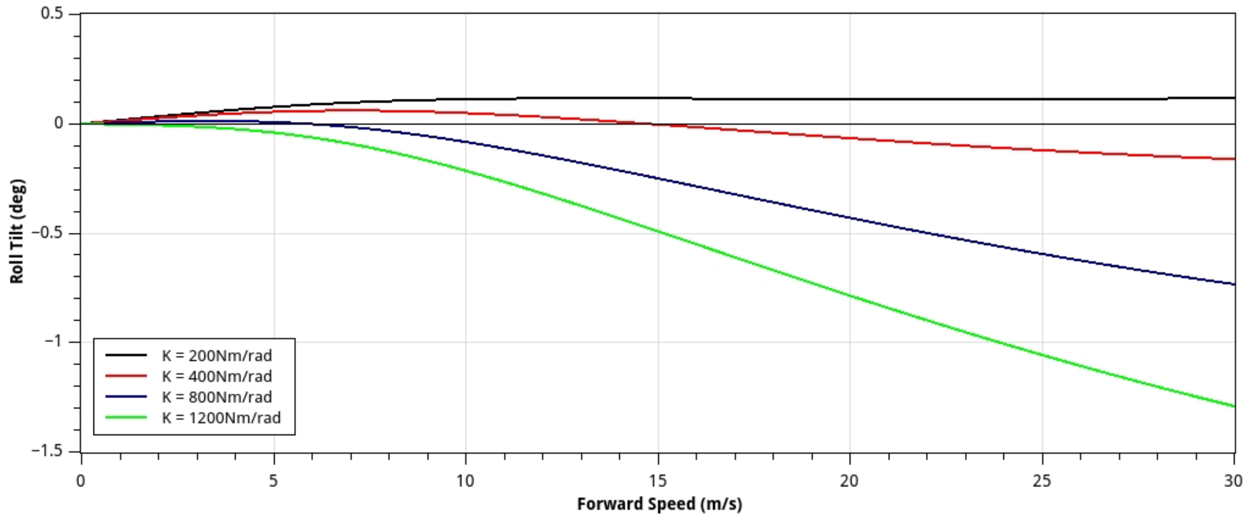


Figure 16: Roll tilt variation in forward flight

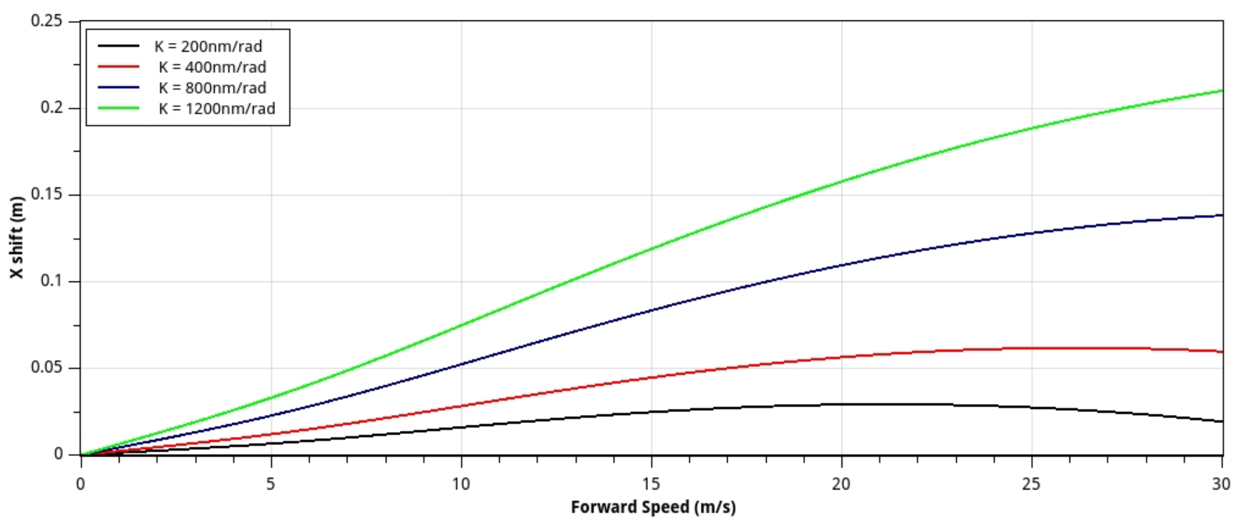


Figure 17: X shift variation in forward flight

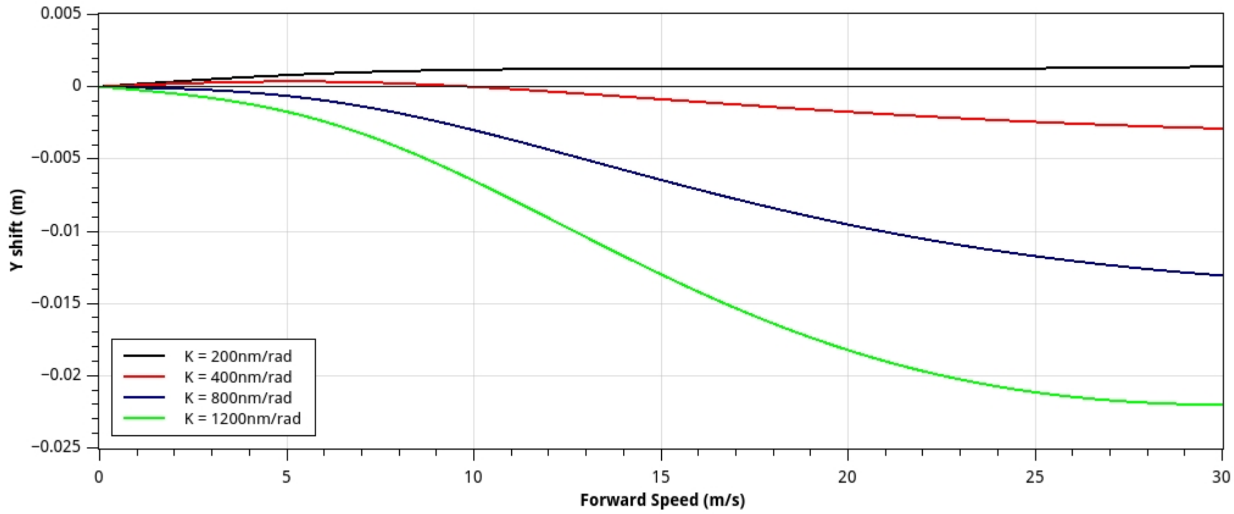


Figure 18: Y shift variation in forward flight

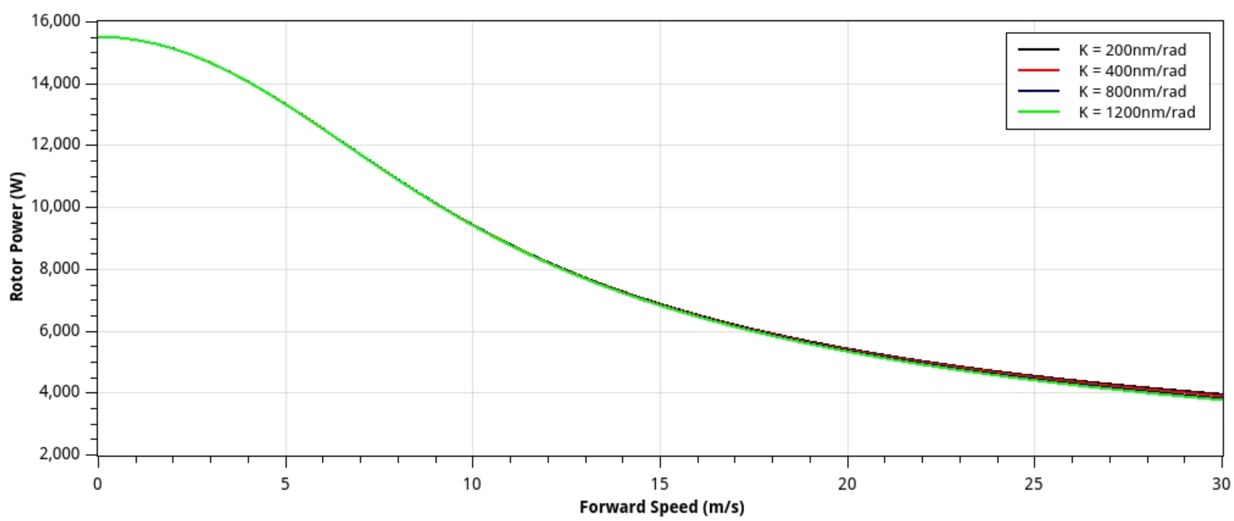


Figure 19: Power variation in forward flight

# 6 Hover Stability and Control Analysis

At hover, the helicopter is assumed to be perfectly vertical. There is no shift in the frame unit and no tilt of the mission unit. The model is shown in Fig. 20.

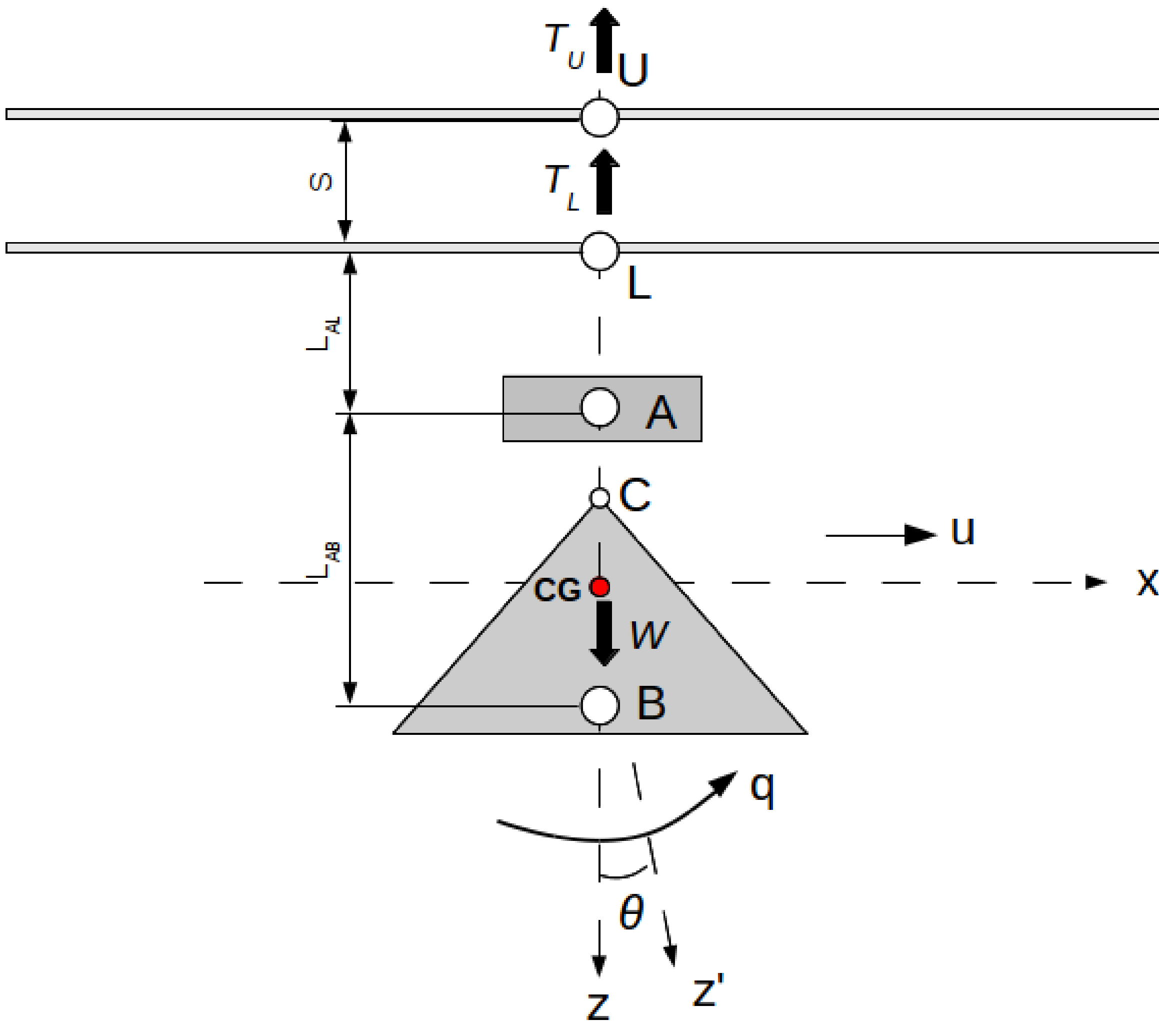


Figure 20: Hover Model

## 6.1 2D Simple Model

At equilibrium, the total thrusts of the rotor are equal to the total weight of the system.

$$(m_A + m_B + m_U + m_L)g = T_{U_o} + T_{L_o} \tag{104}$$

To simplify, the total mass is defined to be: $m_T = m_A + m_B + m_U + m_L$ We now assume that the system is perturbed in the three quantities:

- Forward velocity: $u$
- Pitch Attitude of Vehicle: $\theta$
- Pitch rate of Vehicle: $q$

The equations of motion of the system can be written as:

$$m_T \dot{u} = -m_T g \sin\theta - T_{U_o} \triangle \beta_{1c_u} - T_{L_o} \triangle \beta_{1c_l} \tag{105}$$

$$J_Y \dot{q} = N K_\beta \triangle \beta_{1c_u} + N K_\beta \triangle \beta_{1c_l} + L_{cg-U} T_{U_o} \triangle \beta_{1c_u} + L_{cg-L} T_{L_o} \triangle \beta_{1c_l} \tag{106}$$

The forward force generated is assumed to be due to a tilt of the rotor tip path plane, which corresponds to a change in flap angle coefficient of $\beta_{1c}$.

The net change in moment on the center of gravity comes from two sources for each rotor. One is due to the moment due to blade flap. This is equivalent to the moment on the root spring. The other is due to the moment generated by the forward force of the rotor acting at a distance $L_{cg-U}$ and $L_{cg-L}$ from the center of gravity.

The change in flap angle can be written as:

$$\triangle \beta_{1c} = \frac{\partial \beta_{1c}}{\partial u} u + \frac{\partial \beta_{1c}}{\partial q} q + \frac{\partial \beta_{1c}}{\partial \dot{q}} \dot{q} \tag{107}$$

The derivatives are obtained for a simple rotor model, with a constant chord and blade pitch angle.

$$\frac{\partial \beta_{1c}}{\partial u} = \left( \frac{8}{\Omega R} \right) \left[ \frac{2C_T}{\sigma a} + \frac{\lambda_o}{4} \right] \left( \frac{1}{S_c^2 + 1} \right) \tag{108}$$

Here $C_T$ is the equilibrium thrust coefficient, $\sigma$ is the rotor solidity, $a$ is the lift curve slope, $\lambda_o$ is the rotor inflow and $S_c$ is the coupling parameter. The magnitude of $S_c$ indicates the amount of cross-coupling between the forward and sidewards motion. The cross-coupling parameter is defined as:

$$S_c = \frac{8K_\beta}{\gamma J_b \Omega^2} \tag{109}$$

The lock number $\gamma$ of the blade is given as:

$$\gamma = \frac{\rho a c R^4}{J_b} \tag{110}$$

The derivative with respect to angular motion is

$$\frac{\partial \beta_{1c}}{\partial q} = -\left(\frac{1}{\Omega}\right)\left[\frac{S_c + \frac{16}{\gamma}}{S_c^2 + 1}\right] - \left(\frac{8L_{cg}}{\Omega R}\right)\left[\frac{2C_T}{\sigma a} + \frac{\lambda_o}{4}\right] \tag{111}$$

Similarly, the derivative with respect to rate of angular motion is

$$\frac{\partial \beta_{1c}}{\partial \dot{q}} = -\left(\frac{1}{\Omega^2}\right)\left(\frac{8}{\gamma}\right)\left[\frac{S_c}{S_c^2 + 1}\right] \tag{112}$$

In State-Space form, the equations of motion can be written as:

$$[M]\begin{bmatrix} \dot{u} \\ \dot{q} \\ \dot{\theta} \end{bmatrix} = [K]\begin{bmatrix} u \\ q \\ \theta \end{bmatrix} \tag{113}$$

Where:

$$[M] = \begin{bmatrix} m_T & \left(T_{u_o}\frac{\partial \beta_{1c_u}}{\partial \dot{q}} + T_{l_o}\frac{\partial \beta_{1c_l}}{\partial \dot{q}}\right) & 0 \\ 0 & J_Y - \left(\alpha_u \frac{\partial \beta_{1c_u}}{\partial \dot{q}} + \alpha_l \frac{\partial \beta_{1c_l}}{\partial \dot{q}}\right) & 0 \\ 0 & 0 & 1 \end{bmatrix} \tag{114}$$

and

$$[K] = \begin{bmatrix} -\left(T_{u_o}\frac{\partial \beta_{1c_u}}{\partial u} + T_{l_o}\frac{\partial \beta_{1c_l}}{\partial u}\right) & -\left(T_{u_o}\frac{\partial \beta_{1c_u}}{\partial q} + T_{l_o}\frac{\partial \beta_{1c_l}}{\partial q}\right) & -m_T g \\ \left(\alpha_u \frac{\partial \beta_{1c_u}}{\partial u} + \alpha_l \frac{\partial \beta_{1c_l}}{\partial u}\right) & \left(\alpha_u \frac{\partial \beta_{1c_u}}{\partial q} + \alpha_l \frac{\partial \beta_{1c_l}}{\partial q}\right) & 0 \\ 0 & 1 & 0 \end{bmatrix} \tag{115}$$

Where

$$\alpha = N K_\beta + L_{cg} T_o \tag{116}$$

To solve for the equilibrium conditions we use:

$$T_o = \rho \pi \Omega_o^2 R^4 C_{T_o} \tag{117}$$

and

$$Q_o = \rho \pi \Omega_o^2 R^4 C_{Q_o} \tag{118}$$

The blade element momentum theory with uniform inflow gives us:

$$C_T = \frac{\sigma a}{2}\left(\frac{\theta}{3} - \frac{\lambda}{2}\right) \tag{119}$$

The moment or torque coefficients of each rotor are obtained from:

$$C_q = \kappa C_T \lambda + \frac{\sigma C_{D_o}}{8} \tag{120}$$

The inflow for the lower rotor is assumed to be:

$$\lambda_l = \lambda_{i_l} + k \lambda_{u_i} \frac{\Omega_u}{\Omega_l} \tag{121}$$

Using this for the lower rotor we get:

$$C_{T_l} = \frac{-b - \sqrt{D}}{2} \tag{122}$$

Where:

$$b = -2\left\{C_{T_u} + \frac{\sigma a}{8}\sqrt{\frac{C_{T_u}}{2}}\left(2 - k\frac{\Omega_u}{\Omega_l}\right) + \left(\frac{\sigma a}{8}\right)^2\right\} \tag{123}$$

$$D = 4\left(\frac{\sigma a}{8}\right)^2\left[C_{T_u}\left\{2 + \left(k\frac{\Omega_u}{\Omega_l}\right)^2\right\} + 2\left(\frac{\sigma a}{8}\right)\sqrt{\frac{C_{T_u}}{2}}\left\{2 - \left(k\frac{\Omega_u}{\Omega_l}\right)\right\} + \left(\frac{\sigma a}{8}\right)^2\right] \tag{124}$$

To obtain the hover equilibrium RPM ratio $\bar{\Omega}_o = \frac{\Omega_{u_o}}{\Omega_{l_o}}$, the moment equilibrium equation in non dimensional form reduces to:

$$C_{q_{l_o}} = C_{q_{u_o}} \bar{\Omega}_o^2 \tag{125}$$

As $C_{q_l}$ is also a function of the RPM ratio, the above equation is solved iteratively to obtain the equilibrium RPM ratio of the rotors. Once the equilibrium RPM ratio is known, the thrust equation can be used to obtain the upper and lower rotor neutral RPMs as:

$$\Omega_{l_o} = \sqrt{\frac{m_T g}{\rho \pi R^4 (C_{T_{l_o}} + \bar{\Omega}_o^2 C_{T_{u_o}})}} \tag{126}$$

$$\Omega_{u_o} = \bar{\Omega}_o \Omega_{l_o} \tag{127}$$

The parameters used for this calculation are in Table 6. The value of the average blade pitch angle $\theta$ and the coaxial rotor interference were adjusted to get the rotation speeds close to the ones seen in experiments. The rest of the parameters calculated are given in Table 7. For the given parameters, the equilibrium rotation speeds are $\Omega_{u_o} = 87.64 rad/s$ and $\Omega_{l_o} = 88.13 rad/s$. Given these values, one can also obtain the thrust sharing between the rotors. In the given case, the upper rotor generates 61.8% while the lower rotor generates about 38.1% of the total thrust. The cross-coupling parameter $S_C$ of each rotor was calculated to be:

- $S_{C_u} = 0.172$
- $S_{C_l} = 0.170$

The mass matrix was found to be:

$$[M] = \begin{bmatrix} 166.0 & -0.0745 & 0 \\ 0 & 167.26 & 0 \\ 0 & 0 & 1 \end{bmatrix}$$

and the stiffness matrix was:

$$[K] = 1000.0 \begin{bmatrix} -0.0028 & 0.0820 & -1.6285 \\ 0.0067 & -0.1983 & 0 \\ 0 & 0.001 & 0 \end{bmatrix}$$

The eigenvalues of the system matrix $A = [M]^{-1}.[K]$ were obtained as:

- -1.4016
- 0.0996 + 0.5192 i
- 0.0996 - 0.5192 i

| **Parameter** | **Value** |
|---|---|
| $m_T$ | $166.0kg$ |
| $g$ | $9.81m/s^2$ |
| $N$ | $2$ |
| $K_\beta$ | $645.0Nm/rad$ |
| $L_{AB}$ | $0.899m$ |
| $L_{AL}$ | $0.2m$ |
| $S$ | $0.19m$ |
| $m_B$ | $100.0kg$ |
| $J_b$ | $1.036kgm^2$ |
| $J_B$ | $90.0kgm^2$ |
| $J_A$ | $40.0kgm^2$ |
| $c_0$ | $0.129m$ |
| $c_1$ | $-0.109m$ |
| $R$ | $2.0m$ |
| $L$ | $1.725m$ |
| $R$ | $2.0m$ |
| $\rho$ | $1.205kg/m^3$ |
| $\theta$ | $8.6^o$ |
| $a$ | $5.73/rad$ |
| $k$ | $1.25$ |
| $\kappa$ | $1.15$ |

Table 6: Parameters used for Simulation

| **Parameter** | **Formula** | **Value** |
|---|---|---|
| $A_b$ | $\frac{1}{2}(2c_0 + c_1(L/R))L$ | $0.1414m^2$ |
| $m_r$ | $N(1.17) + 3.7$ | $6.04kg$ |
| $m_A$ | $66.0 - 2m_r$ | $53.92kg$ |
| $\gamma$ | $\frac{\rho a A_b R^2}{J_b}$ | $3.770kgm^2$ |
| $\sigma$ | $\frac{NA_b}{\pi R^2}$ | $0.0225$ |
| $L_{cg-b}$ | $\frac{L_{AB}m_A + (L_{AB}+L_{AL})m_r + (L_{AB}+L_{AL}+S)m_r}{m_T}$ | $0.379m$ |
| $L_{cg-u}$ | $L_{AB} + L_{AL} + S - L_{cg-b}$ | $0.910m$ |
| $L_{cg-l}$ | $L_{AB} + L_{AL} - L_{cg-b}$ | $0.720m$ |
| $L_{cg-a}$ | $L_{AB} - L_{cg-b}$ | $0.520m$ |
| $J_Y$ | $J_B + m_B L_{cg-b}^2 + J_A + m_A L_{cg-a}^2 + m_r L_{cg-l}^2 + m_r L_{cg-u}^2$ | $167.077kg.m^2$ |
| $C_{T_u}$ | $\left[\frac{\sigma a}{8\sqrt{2}} + \sqrt{\frac{\sigma a \theta}{6} + \frac{(\sigma a)^2}{128}}\right]^2$ | $0.00216$ |
| $\lambda_{u_o}$ | $\sqrt{\frac{C_{T_u}}{2}}$ | $0.0329$ |
| $C_{q_u}$ | $\frac{\kappa C_{T_u}^{3/2}}{\sqrt{2}} + \frac{\sigma C_{Do}}{8}$ | $9.884 \times 10^{-5}$ |

Table 7: Calculated Parameters in Simulation

The corresponding eigenvectors were $(u, q, \theta)$:

- $(-0.9752, 0.1802, -0.1286)$
- $(0.9981, -0.0267 + 0.0108i, 0.0105 - 0.0534i)$
- $(0.9981, -0.0267 - 0.0108i, 0.0105 + 0.0534i)$

The positive eigenvalue shows that the vehicle is unstable.

## 6.2 3D Simple Model

The above model was extended to include both roll and pitch motions of the vehicle. This incorporates the coupling between the forward and sideways motion. The equations of motion can now be written as:

$$m_T\dot{u} = -m_T g \sin\theta - T_{U_o} \triangle \beta_{1c_u} - T_{L_o} \triangle \beta_{1c_l} \tag{128}$$

$$m_T\dot{v} = m_T g \sin\phi - T_{U_o} \triangle \beta_{1s_u} - T_{L_o} \triangle \beta_{1s_l} \tag{129}$$

$$J_X\dot{p} = -NK_\beta \triangle \beta_{1s_u} - NK_\beta \triangle \beta_{1s_l} - L_{cg-U}T_{U_o} \triangle \beta_{1s_u} - L_{cg-L}T_{L_o} \triangle \beta_{1s_l} \tag{130}$$

$$J_Y\dot{q} = NK_\beta \triangle \beta_{1c_u} + NK_\beta \triangle \beta_{1c_l} + L_{cg-U}T_{U_o} \triangle \beta_{1c_u} + L_{cg-L}T_{L_o} \triangle \beta_{1c_l} \tag{131}$$

In State-Space form, the equations of motion can be written as:

$$[M]\begin{bmatrix} \dot{u} \\ \dot{v} \\ \dot{p} \\ \dot{q} \\ \dot{\theta} \\ \dot{\phi} \end{bmatrix} = [K]\begin{bmatrix} u \\ v \\ p \\ q \\ \theta \\ \phi \end{bmatrix} \tag{132}$$

Where:

$$[M] = \begin{bmatrix} m_T & 0 & \left(T_{u_o}\frac{\partial\beta_{1c_u}}{\partial\dot{p}} + T_{l_o}\frac{\partial\beta_{1c_l}}{\partial\dot{p}}\right) & \left(T_{u_o}\frac{\partial\beta_{1c_u}}{\partial\dot{q}} + T_{l_o}\frac{\partial\beta_{1c_l}}{\partial\dot{q}}\right) & 0 & 0 \\ 0 & m_T & \left(T_{u_o}\frac{\partial\beta_{1s_u}}{\partial\dot{p}} + T_{l_o}\frac{\partial\beta_{1s_l}}{\partial\dot{p}}\right) & \left(T_{u_o}\frac{\partial\beta_{1s_u}}{\partial\dot{q}} + T_{l_o}\frac{\partial\beta_{1s_l}}{\partial\dot{q}}\right) & 0 & 0 \\ 0 & 0 & J_X + \left(\alpha_u\frac{\partial\beta_{1s_u}}{\partial\dot{p}} + \alpha_l\frac{\partial\beta_{1s_l}}{\partial\dot{p}}\right) & \left(\alpha_u\frac{\partial\beta_{1s_u}}{\partial\dot{q}} + \alpha_l\frac{\partial\beta_{1s_l}}{\partial\dot{q}}\right) & 0 & 0 \\ 0 & 0 & -\left(\alpha_u\frac{\partial\beta_{1c_u}}{\partial\dot{p}} + \alpha_l\frac{\partial\beta_{1c_l}}{\partial\dot{p}}\right) & J_Y - \left(\alpha_u\frac{\partial\beta_{1c_u}}{\partial\dot{q}} + \alpha_l\frac{\partial\beta_{1c_l}}{\partial\dot{q}}\right) & 0 & 0 \\ 0 & 0 & 0 & 0 & 1 & 0 \\ 0 & 0 & 0 & 0 & 0 & 1 \end{bmatrix} \tag{133}$$

and

$$[K] = \begin{bmatrix} K_{11} & K_{12} & K_{13} & K_{14} & -m_T g & 0 \\ K_{21} & K_{22} & K_{23} & K_{24} & 0 & m_T g \\ K_{31} & K_{32} & K_{33} & K_{34} & 0 & 0 \\ K_{41} & K_{42} & K_{43} & K_{44} & 0 & 0 \\ 0 & 0 & 0 & 1 & 0 & 0 \\ 0 & 0 & 1 & 0 & 0 & 0 \end{bmatrix} \tag{134}$$

Where

$$K_{11} = -\left(T_{u_o}\frac{\partial\beta_{1c_u}}{\partial u} + T_{l_o}\frac{\partial\beta_{1c_l}}{\partial u}\right) \tag{135}$$

$$K_{12} = -\left(T_{u_o}\frac{\partial\beta_{1c_u}}{\partial v} + T_{l_o}\frac{\partial\beta_{1c_l}}{\partial v}\right) \tag{136}$$

$$K_{13} = -\left(T_{u_o}\frac{\partial\beta_{1c_u}}{\partial p} + T_{l_o}\frac{\partial\beta_{1c_l}}{\partial p}\right) \tag{137}$$

$$K_{14} = -\left(T_{u_o}\frac{\partial\beta_{1c_u}}{\partial q} + T_{l_o}\frac{\partial\beta_{1c_l}}{\partial q}\right) \tag{138}$$

$$K_{21} = -\left(T_{u_o}\frac{\partial\beta_{1s_u}}{\partial u} + T_{l_o}\frac{\partial\beta_{1s_l}}{\partial u}\right) \tag{139}$$

$$K_{22} = -\left(T_{u_o}\frac{\partial\beta_{1s_u}}{\partial v} + T_{l_o}\frac{\partial\beta_{1s_l}}{\partial v}\right) \tag{140}$$

$$K_{23} = -\left(T_{u_o}\frac{\partial\beta_{1s_u}}{\partial p} + T_{l_o}\frac{\partial\beta_{1s_l}}{\partial p}\right) \tag{141}$$

$$K_{24} = -\left(T_{u_o}\frac{\partial\beta_{1s_u}}{\partial q} + T_{l_o}\frac{\partial\beta_{1s_l}}{\partial q}\right) \tag{142}$$

$$K_{31} = -\left(\alpha_u\frac{\partial\beta_{1s_u}}{\partial u} + \alpha_l\frac{\partial\beta_{1s_l}}{\partial u}\right) \tag{143}$$

$$K_{32} = -\left(\alpha_u\frac{\partial\beta_{1s_u}}{\partial v} + \alpha_l\frac{\partial\beta_{1s_l}}{\partial v}\right) \tag{144}$$

$$K_{33} = -\left(\alpha_u\frac{\partial\beta_{1s_u}}{\partial p} + \alpha_l\frac{\partial\beta_{1s_l}}{\partial p}\right) \tag{145}$$

$$K_{34} = -\left(\alpha_u\frac{\partial\beta_{1s_u}}{\partial q} + \alpha_l\frac{\partial\beta_{1s_l}}{\partial q}\right) \tag{146}$$

$$K_{41} = \left(\alpha_u\frac{\partial\beta_{1c_u}}{\partial u} + \alpha_l\frac{\partial\beta_{1c_l}}{\partial u}\right) \tag{147}$$

$$K_{42} = \left(\alpha_u\frac{\partial\beta_{1c_u}}{\partial v} + \alpha_l\frac{\partial\beta_{1c_l}}{\partial v}\right) \tag{148}$$

$$K_{43} = \left(\alpha_u\frac{\partial\beta_{1c_u}}{\partial p} + \alpha_l\frac{\partial\beta_{1c_l}}{\partial p}\right) \tag{149}$$

$$K_{44} = \left(\alpha_u\frac{\partial\beta_{1c_u}}{\partial q} + \alpha_l\frac{\partial\beta_{1c_l}}{\partial q}\right) \tag{150}$$

The flap angle partial derivatives are obtained to be:

$$\frac{\partial \beta_{1c}}{\partial p} = \frac{\partial \beta_{1s}}{\partial q} = \left(\frac{1}{\Omega}\right)\left[\frac{1 - S_c \frac{16}{\gamma}}{S_c^2 + 1}\right] - \left(\frac{8 S_c L_{cg}}{\Omega R}\right)\left[\frac{2C_T}{\sigma a} + \frac{\lambda_o}{4}\right] \tag{151}$$

$$\frac{\partial \beta_{1c}}{\partial q} = -\frac{\partial \beta_{1s}}{\partial p} = -\left(\frac{1}{\Omega}\right)\left[\frac{S_c + \frac{16}{\gamma}}{S_c^2 + 1}\right] - \left(\frac{8 L_{cg}}{\Omega R}\right)\left[\frac{2C_T}{\sigma a} + \frac{\lambda_o}{4}\right] \tag{152}$$

$$\frac{\partial \beta_{1c}}{\partial \dot{q}} = -\frac{\partial \beta_{1s}}{\partial \dot{p}} = -\left(\frac{1}{\Omega^2}\right)\left(\frac{8}{\gamma}\right)\left[\frac{S_c}{S_c^2 + 1}\right] \tag{153}$$

$$\frac{\partial \beta_{1c}}{\partial \dot{p}} = \frac{\partial \beta_{1s}}{\partial \dot{q}} = \left(\frac{1}{\Omega^2}\right)\left(\frac{8}{\gamma}\right)\left[\frac{1}{S_c^2 + 1}\right] \tag{154}$$

$$\frac{\partial \beta_{1c}}{\partial u} = \frac{\partial \beta_{1s}}{\partial v} = \left(\frac{8}{\Omega R}\right)\left[\frac{2C_T}{\sigma a} + \frac{\lambda_o}{4}\right]\left(\frac{1}{S_c^2 + 1}\right) \tag{155}$$

$$\frac{\partial \beta_{1c}}{\partial v} = -\frac{\partial \beta_{1s}}{\partial u} = -\left(\frac{8}{\Omega R}\right)\left[\frac{2C_T}{\sigma a} + \frac{\lambda_o}{4}\right]\left(\frac{S_c}{S_c^2 + 1}\right) \tag{156}$$

The parameters are strongly dependent on the coupling parameter $S_c$. A small coupling factor is desirable for easier control and stability. Hence blades should have increased elasticity/flexibility and a larger radius. The mass distribution should be such that the inertia of the blade is increased.

The calculated matrices from the above expressions are given as:

$$[M] = \begin{bmatrix} 166 & 0 & 0.4351 & -0.0745 & 0 & 0 \\ 0 & 166 & 0.0745 & 0.04351 & 0 & 0 \\ 0 & 0 & 167.2572 & 1.0533 & 0 & 0 \\ 0 & 0 & -1.0533 & 167.2572 & 0 & 0 \\ 0 & 0 & 0 & 0 & 1 & 0 \\ 0 & 0 & 0 & 0 & 0 & 1 \end{bmatrix}$$

and

$$[K] = 1000.0 \begin{bmatrix} -0.0028 & 0.0005 & -0.0045 & 0.0820 & -1.6285 & 0 \\ -0.0005 & -0.0028 & -0.0820 & -0.0045 & 0 & -1.6285 \\ -0.0011 & -0.0067 & -0.1983 & -0.0110 & 0 & 0 \\ 0.0067 & -0.0011 & 0.0110 & -0.1983 & 0 & 0 \\ 0 & 0 & 0 & 1 & 0 & 0 \\ 0 & 0 & 1 & 0 & 0 & 0 \end{bmatrix}$$

The eigenvalues of the system matrix $A = [M]^{-1}[K]$ are:

- $0.1459 \pm 0.5011i$
- $0.0524 \pm 0.5409i$
- $-1.401 \pm 0.0153i$

The corresponding eigenvectors are: $(u, v, p, q, \theta, \phi)$

- $-0.7058i, 0.7058, -0.0166 + 0.0107i, -0.0107 - 0.0166i, -0.0363 + 0.0108i, 0.0108 + 0.0363i$
- $0.7058i, 0.7058, -0.0166-0.0107i, -0.0107+0.0166i, -0.0363-0.0108i, 0.0108-0.0363i$
- $-0.7057, 0.7057i, -0.0042 - 0.0211i, -0.0211 + 0.0042i, 0.0039 + 0.0394i, -0.0394 + 0.0039i$
- $-0.7057, -0.7057i, -0.0042 + 0.0211i, -0.0211 - 0.0042i, 0.0039 - 0.0394i, -0.0394 - 0.0039i$
- $0.6896, -0.6896i, -0.0026-0.1273i, -0.1273+0.0026i, 0.0909-0.0008i, 0.0008+0.0909i$
- $0.6896, 0.6896i, -0.0026+0.1273i, -0.1273-0.0026i, 0.0909+0.0008i, 0.0008-0.0909i$

The positive real parts of the eigenvalues show that the system is unstable in those modes.

### 6.2.1 Heave Damping

In the heave degree of freedom, there is thrust acting upwards from each of the rotors and the weight of the vehicle acting downwards:

$$m_T \ddot{z} = -T_u - T_l + m_T g \tag{157}$$

Perturbations from equilibrium give us the following equations:

$$m\ddot{\tilde{z}} = -\tilde{T}_u - \tilde{T}_l \tag{158}$$

The perturbation in thrust can be obtained as:

$$\tilde{T}_u + \tilde{T}_l = \rho \pi R^4 \left[ \Omega_{u_o}^2 \tilde{C}_{T_u} + \Omega_{l_o}^2 \tilde{C}_{T_l} \right] \tag{159}$$

$$\tilde{C}_{T_u} = \left(\frac{\partial C_{T_u}}{\partial \dot{\bar{z}}}\right)\dot{\bar{z}} \tag{160}$$

Where

$$\left(\frac{\partial C_{T_u}}{\partial \dot{\bar{z}}}\right) = -\frac{\sigma a}{8}\left[\frac{1}{1+\dfrac{\sigma a}{8\sqrt{2C_{T_{u_o}}}}}\right]\bar{\Omega}_o \tag{161}$$

$$\tilde{C}_{T_l} = \left(\frac{\partial C_{T_l}}{\partial \dot{\bar{z}}}\right)\dot{\bar{z}} \tag{162}$$

The momentum theory gives us the lower rotor inflow as:

$$\lambda_{l_o} = \frac{1}{2}\left[\lambda_{u_o}\left(k\bar{\Omega}_o\right) + \sqrt{\lambda_{u_o}^2\left(k\bar{\Omega}_o\right)^2 + 2C_{T_l}}\right] \tag{163}$$

We need to define a term as shown below:

$$\xi = \frac{2\lambda_{l_o}}{\dfrac{\sigma a}{8} + \sqrt{\lambda_{u_o}^2\left(k\bar{\Omega}_o\right)^2 + 2C_{T_{l_o}}}} \tag{164}$$

Note that:

$$\lambda_{u_o} = \sqrt{\frac{C_{T_{u_o}}}{2}} \tag{165}$$

Another factor is defined as per the following:

$$\eta = \left(\frac{\sigma a + 8\lambda_{u_o}}{\sigma a + 16\lambda_{u_o}}\right) \tag{166}$$

And then we can get the derivatives as:

$$\left(\frac{\partial C_{T_l}}{\partial \dot{\bar{z}}}\right) = -\frac{\sigma a \xi}{8}\left[1 - k\bar{\Omega}_o^2\eta\right] \tag{167}$$

$$\mu\ddot{\bar{z}} = -\left[\bar{\Omega}_o^2\left(\frac{\partial C_{T_u}}{\partial \dot{\bar{z}}}\right) + \left(\frac{\partial C_{T_l}}{\partial \dot{\bar{z}}}\right)\right]\dot{\bar{z}} \tag{168}$$

The mass factor is given as:

$$\mu = \frac{m_T}{\rho \pi R^3} \tag{169}$$

In dimensional form:

$$\dot{w} = -\left(\frac{1}{\mu\Omega_{l_o}}\right)\left[\Omega_{u_o}^2\left(\frac{\partial C_{T_u}}{\partial \dot{\hat{z}}}\right) + \Omega_{l_o}^2\left(\frac{\partial C_{T_l}}{\partial \dot{\hat{z}}}\right)\right] w \tag{170}$$

After calculating using the previous parameters:

$$\dot{w} = -0.2927w$$

## 6.3 Control Analysis

For the hover state, the following four control inputs are identified:

1. Tilt Forward of Mission Unit $\delta_\theta$
2. Tilt Side-ward of Mission Unit $\delta_\phi$
3. Shift Forward of Frame Unit $X_{shift}$
4. Shift Side-ward of Frame Unit $Y_{shift}$

The contribution of the tilt is only to the forward and side-ward forces only, while the shift creates a moment about the center of gravity. The complete dynamic equations can be written as:

$$[M]\begin{bmatrix}\dot{u}\\ \dot{v}\\ \dot{p}\\ \dot{q}\\ \dot{\theta}\\ \dot{\phi}\end{bmatrix} = [K]\begin{bmatrix}u\\ v\\ p\\ q\\ \theta\\ \phi\end{bmatrix} + [C]\begin{bmatrix}\delta_\theta\\ \delta_\phi\\ X_{shift}\\ Y_{shift}\end{bmatrix} \tag{171}$$

The control matrix is found to be:

$$[C] = \begin{bmatrix} m_T g & 0 & 0 & 0\\ 0 & m_T g & 0 & 0\\ 0 & 0 & 0 & m_B\left(2-\frac{m_B}{m_T}\right)g\\ 0 & 0 & -m_B\left(2-\frac{m_B}{m_T}\right)g & 0\\ 0 & 0 & 0 & 0\\ 0 & 0 & 0 & 0 \end{bmatrix} \tag{172}$$

After the calculation, we obtain:

$$[C] = \begin{bmatrix} 1628.5 & 0 & 0 & 0 \\ 0 & 1628.5 & 0 & 0 \\ 0 & 0 & 0 & 1371.0 \\ 0 & 0 & -1371.0 & 0 \\ 0 & 0 & 0 & 0 \\ 0 & 0 & 0 & 0 \end{bmatrix}$$

The controllability of the system can be found by comparing the rank of the system matrix and the controllability matrix, which for the current calculation, turns out to be 6 for both. Hence the system is unstable, yet controllable in hover.

# 7 Conclusions

## 7.1 Results

The following are the key conclusions of the study:

- The blade mass distribution and geometry plays a key role in the rotor flapping behavior.
- The finite element analysis can help predict the mass and stiffness distribution for a required spring constant.
- The rotor aerodynamics accounts for the linear taper and twist, so can be used to design new blades.
- The forward flight results show that the spring constant determines the cross-coupling behavior of the rotor at forward flight.
- The blade flapping causes large oscillatory loads on the vehicle.
- The vehicle is unstable in hover, but controllable.

## 7.2 Future Work

The following are some areas which need to be addressed in the future:

- The stability and control analysis should be extended for forward flight and general maneuvers.
- The rotor hub forces and moments should be made more accurate to account for reverse stall and inflow so that the simulation matches more accurately.
- The inflow model needs to account for the inertia of the air. This can be approximated by using a low pass filter.
- The rotor model should also include the rotation speed of the hub as well.
- The current analysis uses a quasi static approach for the aerodynamic forces. Using unsteady aerodynamics for the blades will improve the prediction of rotor loads.

- Experiments with less stiff blades will be useful to match simulation results.
- Experiments with a smaller fixed pitch and faster rotors need to be done.
- The control mechanism will benefit with a power steering or fly by wire system due to the very small control inputs required in the shift and tilt in forward flight.
- The blade aerodynamic cross-section can be optimized to increase forward flight. The sections close to the root should have high stall angles, while the sections near the tip should have high lift to drag ratios.
- According to the requirements of the GEN corporation, a full mathematical model of the vehicle will be useful to get characteristics such as Autorotation capability and predict handling and flying qualities in all maneuvers.